

1 Response to Referee #1

2

3 **Introduction**

4 We thank referee #1 for a close reading of this manuscript and suggestions for
5 improvement. In the following, we explain how we have addressed the reviewer's
6 comments (comments in blue, responses in black). We refer to actual changes in the main
7 text using primarily the original page/line numbers in the downloadable pdf-file on the
8 interactive discussion webpage; in italics, we have also included the corresponding
9 page/line numbers in the updated .pdf-file, uploaded separately. We summarize
10 additional information from several new figures added to the supplement: one set of
11 figures showing $>51 \mu\text{m}$ POC:²³⁴Th, PIC:²³⁴Th and BSi:²³⁴Th profiles at all stations (Fig.
12 S1), and three figures synthesizing phytoplankton cell count data from co-author Barney
13 Balch (Figs., 2, 3 and 4). The changes in main text and supplement are appended after
14 these responses.

15

16 **Comment 1.** The authors fit the classic power-law curve of Martin et al. to their flux
17 profiles. As they point out, this requires some careful thought about the relevant
18 export depth. To avoid this, and to make comparison between stations simpler, an
19 alternative is the exponential fit of Buesseler and Boyd (2009, L&O). If one
20 makes the assumption that sinking speed is constant with depth, the estimate of
21 remineralisation length scale is independent of choice of export depth (see e.g.
22 Marsay et al., 2015, PNAS). Of course, the authors would have to check whether
23 the exponential fit was robust for their data. In the discussion (page 2869), the
24 authors actually switch to a discussion of remineralisation length scale which is
25 inconsistent with the use of transfer efficiency and 'b' up to that point. Perhaps
26 reframing the manuscript in terms of remineralisation length scale would be
27 useful?

28 In Section 4.7, we use the term "remineralization length-scale" to conceptually
29 differentiate POC transfer from BSi-rich (page 2868, lines 18-19) and PIC-rich stations
30 (page 2869, line 20) across GB1 and GB2. We agree with the reviewer that this
31 conceptual use of the term can be erroneously associated with an exponential [POC]

32 profile fit, which we do not apply to the POC flux or $>51 \mu\text{m}$ POC concentration profiles
33 in this manuscript. Therefore, we have removed this term from those two particular parts
34 of Section 4.7.

35 We have decided to continue using power law-derived attenuation coefficients
36 and transfer efficiency (T_{100} , or the ratio of POC flux 100 m below z_{PAR} to POC flux at
37 z_{PAR}) to describe POC transfer in the mesopelagic zone throughout Section 4. Because we
38 measured $>51 \mu\text{m}$ [POC] up to 1000 m in depth, a power-law fit would be superior to a
39 single exponential fit, while an exponential fit would work best above ~ 300 m (Lam and
40 Bishop, 2007, Deep Sea Research II; Buesseler and Boyd, 2009, Limnology and
41 Oceanography). Moreover, fitting $>51 \mu\text{m}$ [POC] profiles to a power law is conceptually
42 significant because it assumes that, at steady-state, [POC] at a given depth is only
43 governed by the sinking flux and loss due to remineralization and particle disaggregation,
44 and that these loss rates are depth-dependent (Lam and Bishop, 2007, Deep Sea Research
45 Part II). Similarly, we focus on T_{100} , as defined in Buesseler and Boyd (2009), to describe
46 POC flux changes from a consistently defined export depth in the most dynamic depth
47 range below the euphotic zone.

48

49 **Comment 2.** The paper provides some interesting particle composition data, which
50 are used to explain trends in POC flux and suggest a strong role of ecosystem
51 structure. It would be beneficial to the interpretation to include more information
52 on the phytoplankton community composition in the study regions (using past
53 studies if in situ data concurrent with sampling are not available). This would
54 provide further weight to the explanations hypothesised by the authors. A plot
55 showing diatom vs coccolithophore dominated regions based on PIC and BSi
56 ratios could be a useful addition.

57 We agree with reviewer #1 that more information on the phytoplankton community at all
58 stations across GB1 and GB2 would strengthen our hypotheses connecting ecosystem
59 composition to POC transfer, which are currently based on $>51 \mu\text{m}$ BSi and PIC
60 concentrations. To address this, we compared our [BSi] and [PIC] measurements to
61 coccolithophore and diatom cell counts measured by co-author Barney Balch at
62 corresponding stations and have added 3 supplementary figures (Figs. S2, S3, S4). The

63 comparisons show that total coccolithophores and diatoms in the euphotic zone are
64 significantly and positively correlated with $>51 \mu\text{m}$ [PIC] and [BSi] at Z_{PAR} , respectively
65 ($p < 0.05$). This supports our use of biomineral concentrations to infer phytoplankton
66 community structure across the Great Calcite Belt. The caveats of this comparison and
67 methodology involved in the phytoplankton cell counts are discussed in the supplement.

68 We now refer to these supplementary figures in the main text, Section 4.7 (pages
69 2867, 2868 {pages 24-25}), where we discuss ecosystem composition in terms of $>51 \mu\text{m}$
70 [BSi] and [PIC] measurements, and in the Fig. 10 caption. Notably, Fig. S4 demonstrates
71 that several stations which we have interpreted to be “diatom-dominated” because >51
72 μm [PIC]:[BSi] < 1 (e.g., page 2868, lines 9-11) exhibit more coccolithophore than diatom
73 cell counts in the euphotic zone. Even though this may be due to the different size
74 fractions that are being compared, this observation has persuaded us to reword our
75 descriptions of stations as “dominated” by coccolithophores (if [PIC]:[BSi] > 1) or
76 diatoms (if [PIC]:[BSi] < 1) in Section 4.7. Instead, we describe such stations as either
77 exhibiting higher “relative abundances” of coccolithophores (if [PIC]:[BSi] > 1) or
78 diatoms (if [PIC]:[BSi] < 1) in the euphotic zone.

79

80 **Comment 3.** The authors have collected a wealth of data on particle
81 composition with depth. It would be beneficial to show profiles of ratios of Th
82 with POC, PIC, and BSi to give an idea of the variability with depth and hence
83 how appropriate the choice of the ratio at a depth of Z_{PAR} is for calculating the
84 export flux. This information could perhaps be included in supplementary
85 information.

86 We have added a four-part supplementary Fig. S1, which shows profiles of all $>51 \mu\text{m}$
87 POC: ^{234}Th , PIC: ^{234}Th and BSi: ^{234}Th measurements at each station. The panels also
88 indicate depths corresponding to Z_{PAR} , $Z_{\text{Th/U}}$ and, for POC: ^{234}Th , 100 m below Z_{PAR} . Note
89 that the PIC: ^{234}Th and BSi: ^{234}Th profiles do not extend far below the euphotic zone
90 because there are fewer $>51 \mu\text{m}$ [PIC] and [BSi] measurements at such depths. We have
91 modified section 2.3 to reflect this. Moreover, although the PIC: ^{234}Th and BSi: ^{234}Th
92 panels do not show interpolated values at $Z_{\text{Th/U}}$, the measurements available should give
93 readers a sense of how variable these metrics are at depths close to $Z_{\text{Th/U}}$, and how

94 choosing $z_{Th/U}$ as an export depth would hypothetically influence the PIC: ^{234}Th and BSi:
95 ^{234}Th values used in biomineral export flux calculations. We add a reference to Fig. S1 in
96 Sect. 3 (page 2856, line 22 *{line 373}*) and Sect. 4.4 (page 2862, line 21 *{line 550}*).

97
98 **Comment 4.** Page 2845, line 3: replace “~1000 m” with “(from the base of the
99 euphotic zone to ~1000 m)”

100 Changed on page 2845, line 3 *{line 46}*.

101

102 **Comment 5.** Page 2845, line 8: add reference (maybe Kwon et
103 al. 2009 Nature)

104 We added this reference on page 2845, line 8 *{line 51}*.

105

106 **Comment 6.** Page 2845, line 25: replace “remaining intact on its way down”, with
107 “reaching the deep ocean”

108 Changed on page 2845, line 25 *{line 68}*.

109

110 **Comment 7.** Page 2848, line 21: give duration of pumping and volume
111 of water pumped

112 We included this information in an additional sentence on page on 2848, line 28 *{lines*
113 *160-161}*.

114

115 **Comment 8.** Page 2849, line 27: give duration
116 of acid fuming

117 Added detail on page 2849, line 27 *{line 191}*.

118

119 **Comment 9.** Page 2850, line 11-13: ‘We focus our assumption.because we
120 assume they contribute disproportionately to sinking fluxes’. Are the authors able
121 to test this assumption with their dataset? The <51um data which were collected
122 do not seem to be used in the manuscript?

123 We are not able to test this assumption with the data available, as we would need
124 measurements of the size distribution of actual sinking particles collected by sediment

125 traps, but no sediment traps were deployed on these cruises. The $<51 \mu\text{m}$ [POC]
126 measurements are used in calculating the fraction of [POC] that is in the $>51 \mu\text{m}$ size-
127 fraction. We use this metric in the discussion to discuss the association between $>51 \mu\text{m}$
128 [BSi] at z_{PAR} , the $>51 \mu\text{m}$ [POC] attenuation coefficient and particle size distribution
129 (Sect. 4.7, Fig. 10).

130

131 **Comment 10.** Page 2853, line 4: Why is the 0.3% light level chosen to
132 represent euphotic depth, when it is more commonly defined as 1%?

133 The Niskin bottles were tripped at depths corresponding to light levels in incubation
134 experiments being conducted on board (Balch et al., in prep). The screening used for the
135 incubation experiments was approximately 0.3% surface PAR, and so this is the light
136 level at which the Niskins were tripped. We have added a line to section 2.1 (page 2848,
137 line 8 *{lines 136-137}*) to explain this. Because most export flux studies use export
138 depths corresponding to light levels between 0.1% and 1% PAR (e.g., Jerlov, 1968;
139 Poulton et al., 2006, Global Biogeochemical Cycles; Buesseler and Boyd, 2009,
140 Limnology and Oceanography), we found it appropriate to choose depths at 0.3% PAR
141 in order to keep our data set consistent with other depth-specific measurements from the
142 Niskin casts.

143

144 **Comment 11.** Page 2854, line 4-6: The authors should identify somewhere (one of
145 the tables?) which stations did not show a classic Martin curve.

146 In Table 2, we indicate which stations did not exhibit a significant Martin curve for >51
147 μm [POC] by writing “no fit” into the corresponding row of column four (titled, “ >51
148 μm [POC] attenuation”). As we do not use Martin curve fits of $<51 \mu\text{m}$ [POC] profiles in
149 this manuscript, we do not report the attenuation coefficients or significance of these fits
150 in Table 2.

151

152 **Comment 12.** Page 2858: The authors use ‘productivity’ or ‘primary productivity’
153 when they mean (satellite-derived) ‘chlorophyll’.

154 On page 2858 *{page 15}*, we have replaced “productivity” with “chlorophyll”.

155

156 **Comment 13.** Page 2859, line 23-27: could be worth tabulating these data from
157 other studies to allow reader to easily compare
158 We decided not to tabulate these ²³⁴Th and POC flux measurements, originally compiled
159 in Le Moigne et al. (2013, Earth System Science Data), because the table would have
160 over two-hundred entries. We added a clarification on line 23 of page 2859 *{page 16,*
161 *line 462}* that all the data from other the citations on lines 23-27 are included in this
162 compilation. Instead of tabulating these data, we decide to report the mean and standard
163 deviation of all the compiled fluxes alongside the mean and standard deviation of the
164 fluxes from GB1 and GB2 on lines 22-28 *{lines 460-468}*.

165

166 **Comment 14.** Page 2861, lines 14-16: Maiti et al. actually showed a strong
167 correspondence between PP and export (just the direction of the relationship was
168 opposite to previous studies).

169 We corrected an error in the reference here on page 2861 line 16 *{line 516}*, which
170 should read “Maiti et al., 2012” rather than “Maiti et al., 2010.” Maiti et al. (2012, Deep
171 Sea Research Part II) report ²³⁴Th-derived POC export fluxes from a highly productive
172 eddy in the Central Pacific through the decline of a diatom bloom, as well as from a site
173 west of the eddy influence. Contrary to the hypothesis that such high-productivity eddies
174 export proportional amounts of carbon, they found that there was no correlation between
175 primary productivity and POC export in the eddy, and no difference in export efficiency
176 between the eddy site and non-eddy site. For this reason, we find it appropriate to cite
177 Maiti et al. (2012) here when commenting on the lack of correlation between primary
178 productivity and POC export in our dataset.

179

180 **Comment 15.** Page 2862, discussion of $T_{100}>1$ values: if the sampling took place
181 post-bloom, when PP is declining but export is still high, this may result in ratios
182 >1 , i.e. non steady state (Henson et al. 2015, GBC).

183 We acknowledge that sampling after a bloom/during bloom decline could decouple
184 phytoplankton and zooplankton-driven particle export (Henson et al., 2015, Global
185 Biogeochemical Cycles), generating higher POC fluxes below the export depth and
186 causing $T_{100}>1$. However, there is no evidence from the satellite chlorophyll imagery

187 that sampling for those five particular stations with $T_{100}>1$ took place during a bloom
188 decline. We have added a sentence to page 2862, line 8 *{lines 535-537}* to reflect this.

189

190 **Comment 16.** Page 2862, line 25: Are the authors able to specify the
191 “sampling issue”?

192 We do not have an explanation for why the POC:²³⁴Th at GB1-25 increases, but note
193 that this station had the lowest attenuation of POC (Table 2) and is the only station
194 where POC: ²³⁴Th consistently increases with depth in the upper 400 m. Poor particle
195 distributions on prefilters around the depth of Z_{PAR} at GB2-106 may explain the
196 increasing POC: ²³⁴Th below Z_{PAR} (Fig S1b). We have added a sentence to page 2862,
197 line 25 *{lines 553-556}* that reflect this.

198

199 **Comment 17.** Page 2864, line 20-24: sentence could be made clearer, also
200 repeated “2.199”?

201 We clarified the wording on lines 20-24 of page 2864 *{lines 610-614}*, and deleted
202 the extra “2.199”.

203

204 **Comment 18.** Page 2867, line 1: “further strengthening”... Do the fits of any of
205 the other stations improve if only looking at upper 500 m? If attenuation over
206 only upper 500 m was plotted against [BSi] and [POC], is a higher correlation
207 observed?

208 There are only eight stations with $>51 \mu\text{m}$ [POC] profiles that fit significantly ($p<0.05$)
209 to a Martin curve between Z_{PAR} and 500 m, including GB1-85, compared with 21
210 stations that do significantly fit to a Martin curve between Z_{PAR} and 800-1000 m. For
211 these 8 stations, the correlation between these upper 500 m b-values and $>51 \mu\text{m}$
212 [BSi] at Z_{PAR} is stronger ($r^2=0.53$ compared to $r^2=0.35$ in Fig. 10a). However, this
213 correlation is weaker than when only the 500 m b-value at GB1-85 is included in the
214 regression and all the other 20 b-values are from fits to deep $>51 \mu\text{m}$ [POC] ($r^2=0.60$)
215 (dashed line in Fig. 10a). Thus, we do not find this 8-point regression to strengthen the
216 association between $>51 \mu\text{m}$ [BSi] and POC transfer in the mesopelagic zone.

217 There is no correlation between these eight upper 500 m b-values and % >51
218 μm [POC] at z_{PAR} .

219

220 **Comment 19.** Page 2868, line 22: what is the ‘model diatom community’?

221 On line 22, the “model diatom community” refers to diatom-dominated communities
222 that efficiently export large, BSi- and POC-rich aggregates out of the euphotic zone,
223 as we describe on page 2867, lines 7-10 (Michaels and Silver, 1998, Deep Sea
224 Research; Buesseler 1998, Global Biogeochemical Cycles; Thomalla et al., 2006,
225 Deep Sea Research Part II). We discuss GB1-85 as a model diatom community in the
226 previous paragraph on page 2868, starting at line 8. We decided to add some text to
227 clarify this on line 22 of page 2868 *{line 724}*.

228

229 **Comment 20.** Page 2879, line 1-5: Figure 10b does not show a clear
230 separation of diatom versus coccolithophore-dominated regions. Is there any
231 statistical significance in the difference attenuation coefficients for these two
232 regions (based on [PIC]:[BSi])? It could be worth plotting regression lines in
233 figure 10b, for only diatom-dominated and only coccolithophore-dominated
234 regions. The plot suggests that there would be no relationship between
235 attenuation coefficient and %>51 μm POC for coccolithophore- dominated
236 regions.

237 According to the Student’s *t*-test, attenuation coefficients at stations with >51 μm
238 [PIC]:[BSi]>1 at z_{PAR} are not significantly different from attenuation coefficients at
239 stations with [PIC]:[BSi]<1. The reviewer is correct that there is no significant
240 correlation between attenuation coefficient and % >51 μm [POC] at z_{PAR} for stations
241 where [PIC]:[BSi]>1, which is why we choose to represent the natural log of [PIC]:[BSi]
242 as a color bar in Fig. 10 rather than an axis. We find this color bar representation useful
243 for highlighting where particular stations with relatively more >51 μm [PIC] than [BSi]
244 at z_{PAR} , and vice-versa, would fall along the axes in panels a and b. As we elaborate in
245 Sect. 4.7, the information from the color bar points to some relationship between
246 phytoplankton community composition and the attenuation of >51 μm [POC] in the
247 mesopelagic zone.

248

249 **Comment 21.** Page 2879, line 12-23: Could the differences in dissolution rates
250 of PIC and BSi explain the differences in attenuation for the regions dominated
251 by diatoms vs coccolithophores?

252 Yes, differences in dissolution rates of the two biominerals could confound the
253 relationships we discuss in Fig. 10. But, as stated on page 2870, lines 17-20,
254 there was no association between the magnitude of $>51 \mu\text{m}$ [PIC]:[BSi] change
255 with depth and attenuation. If different dissolution rates systematically biased
256 the relationships in Fig. 10, then we would expect attenuation to scale with these
257 changes in biomineral ratios with depth.

258

259 **Comment 22.** Page 2879, line 21: [PIC]: [Si], should be [BSi]?

260 Changed on page 2870, line 12 *{line 771}*.

261

262 **Comment 23.** Table 2: Is b calculated from Z_{PAR} to $Z_{\text{PAR}} + 100$, or deeper? Is it
263 calculated from > 2 data points? Does the deep transfer efficiency (e.g. POC at
264 $\sim 800\text{m}$ /POC at Z_{PAR}) add anything useful to the discussion? Does ‘no fit’ mean
265 that the fit was not statistically significant? At what level?

266 The attenuation coefficient, or b-value, is calculated from Z_{PAR} to the deepest $>51 \mu\text{m}$
267 [POC] measurement (800-1000 m), which includes more than two points. We added a
268 clarification to page 2850, lines 2-6 *{lines 195-196}*. In addition, we added a footnote to
269 Table 2 explaining that no fit means that the Martin curve fit was not statistically
270 significant ($p>0.05$).

271 It is not possible to calculate a deep transfer efficiency in terms of POC fluxes
272 because ^{234}Th -derived POC flux calculations do not extend to 800 – 1000 m, as there
273 were no ^{234}Th - ^{238}U disequilibria at such depths. In terms of concentration, the
274 quotient $>51 \mu\text{m}$ [POC] at 800 m/[POC] at Z_{PAR} is analogous and significantly correlated
275 to the attenuation coefficient ($p=1\text{E-}05$, $r^2=0.67$). Therefore, b values are sufficient for
276 the purposes of our discussion, and it is not necessary to add another “deep transfer
277 efficiency” metric.

278

279 **Comment 24.** Figures 1, 5, 6 and 8: Would it be possible to use more precise front
280 positions e.g. Orsi et al 1995, Thorpe et al. 2002?

281 We recognize that the single latitude front positions we've drawn in figures 1, 5, 6, 8 are
282 extremely simplistic, and that a more nuanced categorization based on more
283 hydrographic parameters would be far more accurate. However, Fig. 1 shows surface
284 temperature relative to our simplistic Subtropical, Subantarctic and Polar front positions,
285 and it can be seen that these provide a reasonable grouping of stations by temperature
286 range. As we primarily use these front positions as a way to facilitate data description in
287 Sect. 3 (pages 2855-2856) and Table 4, we decided to keep our simplistic zonations.

288

289 **Comment 25.** Figures 5-8: Is it area or diameter of circle which corresponds to
290 flux? Difficult to see spatial trends from these figures.

291 We have included some text in the Figs. 5-8 captions to clarify that the area of the circle
292 corresponds to the value displayed in the legend. We find that this is best geographical
293 representation of the different measurements we discuss in the manuscript. More precise
294 values of these measurements are provided in Tables 2 and 3.

295

296 **Comment 26.** Figure 2: I found it very hard to distinguish the different particle
297 types in this photos – possible just the quality of my printout!

298 In an attempt to improve the image quality, we imported the images as .tif-files into
299 Adobe Photoshop and applied various image quality adjustments (i.e., sharpening and
300 contrast) and saved them together as an .eps-file. The image is still quite pixelated
301 despite these improvements, but this is the best improvement that is possible with the
302 images that we have. We will re-submit this improved image as Fig. 2, and have
303 shown it above the Fig. 2 caption in the appended track changes section of this
304 response below.

305 We have added some text in the Fig. 2 caption to direct readers to specific important
306 features in the different panels (e.g., cylindrical fecal pellets in panel c).

307

308 **Comment 27.** Figure 4: very long, lots of info, and not sure it's needed in the main
309 text – could this be moved to supplementary?

310 We have decided to keep Fig. 4 in the main text because it plays a large role in the
311 results and discussion sections of the manuscript. In particular, we discuss the ^{234}Th
312 activity profiles extensively (Sect. 3 and Sect. 4.1) to assess how the choice of export
313 depth (Z_{PAR} vs. $Z_{\text{Th/U}}$) impacts the ^{234}Th -derived fluxes we report in the rest of the
314 results/discussion.

315

316 **Comment 28.** Figure 9B and 10B: the regressions seem to be very much driven by
317 station GB1-85 which appears to be an outlier. Did the authors test whether the
318 relationships remain statistically significant if this data point was excluded?

319 In Fig. 9b, the relationship remains statistically significant if GB1-85 is removed from
320 the regression, as discussed on page 2864, line 10. Likewise, in Fig. 10b, the correlation
321 remains significant ($p \ll 0.05$) when excluding GB1-85, as discussed on page 2866, lines
322 20 - 21.

323

324 Response to Referee #2

325

326 We thank referee #2 for thorough comments and clear suggestions for improvement.
327 Here we discuss information from several new supplemental figures that synthesize
328 ecosystem composition data with our particulate bulk concentration measurements at
329 corresponding stations in the Great Calcite Belt cruises. We refer to the changes made in
330 the manuscript using the original page/line numbers in the downloadable pdf-file on the
331 interactive discussion webpage. To see the actual changes in main text and supplement,
332 please refer to what we have appended to our response to referee #1.

333

334 We found that in responding to referee #1's first comment, we were able to address
335 referee #2's main suggestions for improvement. Referee #2 wrote:

336

337 "I only have one minor comment related to the impact of the plankton community
338 composition of POC export and remineralization. The authors present a large and well
339 synthesize dataset of particle export but this paper is very 'particle centric'. Indeed, I
340 would have liked to see external data to confort their conclusions on the impact of the
341 plankton community composition on POC export that is only based on BSi and PIC
342 fluxes in this study. Is there any external data available (HPLC pigments, phytoplankton
343 compositions from slides/cytometry, remote sensing estimations of phytoplankton
344 composition such as PHYSAT and others ...)?"

345

346 We agree that more information on the phytoplankton community at all stations across
347 GB1 and GB2 would strengthen our hypotheses connecting ecosystem composition to
348 POC transfer, which are currently based on $>51 \mu\text{m}$ BSi and PIC concentrations. To
349 address this, we compared our [BSi] and [PIC] measurements to coccolithophore and
350 diatom cell counts measured by co-author Barney Balch at corresponding stations and
351 have added 3 supplementary figures (Figs. S2, S3, S4). The comparisons show that total
352 coccolithophores and diatoms in the euphotic zone are significantly and positively
353 correlated with $>51 \mu\text{m}$ [PIC] and [BSi] at Z_{PAR} , respectively ($p < 0.05$). This supports our
354 use of biomineral concentrations to infer phytoplankton community structure across the

355 Great Calcite Belt. The caveats of this comparison and methodology involved in the
356 phytoplankton cell counts are discussed in the supplement.

357 We now refer to these supplementary figures in the main text, Section 4.7 (pages
358 2867, 2868), where we discuss ecosystem composition in terms of $>51 \mu\text{m}$ [BSi] and
359 [PIC] measurements, and in the Fig. 10 caption. Notably, Fig. S4 demonstrates that
360 several stations which we have interpreted to be “diatom-dominated” because $>51 \mu\text{m}$
361 [PIC]:[BSi] <1 (e.g., page 2868, lines 9-11) exhibit more coccolithophore than diatom cell
362 counts in the euphotic zone. Even though this may be due to the different size fractions
363 that are being compared, this observation has persuaded us to reword our descriptions of
364 stations as “dominated” by coccolithophores (if [PIC]:[BSi] >1) or diatoms (if
365 [PIC]:[BSi] <1) in Section 4.7. Instead, we describe such stations as either exhibiting
366 higher “relative abundances” of coccolithophores (if [PIC]:[BSi] >1) or diatoms (if
367 [PIC]:[BSi] <1) in the euphotic zone.

368

369

370 Summary of changes in manuscript

371

372

1. Abstract

373

Line 30: changed “diatom-dominated” to “diatom-rich”.

374

2. Introduction

375

Line 46: changed “~1000m” to “(from the base of the euphotic zone to ~1000 m)”.

376

377

Line 51: added reference (Kwon et al., 2009).

378

Line 68: replaced “remaining intact on its way down” with “reaching the deep

379

sea”.

380

3. Methods

381

Line 136: added “to match light levels in deck-board incubators” after “surface irradiance”.

382

383

Line 160: added a sentence, “An average of 200 L and 500 L of seawater passed

384

through the Supor and QMA flow paths over 1-2.5 hours, respectively.”

385

Line 184: Deleted “and depth” at end of sentence. Then, added a sentence, “POC concentrations were measured at all depths of the profiles, while [PIC] and [BSi] were mainly measured at select depths above 200 m and at the deepest depth (800-1000 m) of the profile.”

386

387

388

Line 191: added “overnight (12-17 hours)” between the words “fumed” and

389

“with”.

390

Line 195: replaced “below the euphotic zone” with “between the base of the euphotic zone and the deepest measurement at 800 – 1000 m”.

392

393

Line 201: replaced “active” with “available”.

394

4. Results

395

Line 373: added reference to Fig. S1 at end of sentence.

396

Lines 422-430: replaced words “productivity” or “primary productivity” with either “chlorophyll” or “chlorophyll concentrations.”

397

398

Line 425: replaced word “experienced” with “exhibited”.

399

Line 431: added “-series” to word “time”.

400

Lines 460-461, 467-468: added means and standard deviation values of fluxes.

401

Line 461: added “compilation by” before first in parentheses.

402

Line 516: changed year of Maiti et al. reference from 2010 to 2012.

403

Line 535: added sentence, “Transfer efficiencies greater than 1 can occur during a declining bloom (Henson et al., 2015), but examination of satellite chlorophyll time-series does not indicate that these stations were sampled at such conditions.”

404

405

Line 550: added reference to supplementary Fig. S1.

406

Line 552: added word “at” after “this is unexpected and”. Deleted “where”.

407

Lines 553: replaced last sentence of paragraph with “We suspect that poor >51

408

µm particle distribution on filters from GB2-106 may have led to anomalously low POC around Z_{PAR} , but do not have an explanation for the consistent increase

409

in POC:Th with depth at GB1-25 (Figs. S1a). We proceed by excluding the T_{100}

410

transfer efficiencies from these two stations from statistical tests, but identify

411

them for completeness (Figs. 7, 9).”

412

Lines 610-614: reworded the sentences on these lines to be more clear. Also

413

deleted extra “x 2.199”.

414

415

416 Lines 676-783: reworded any phrasing referring to a coccolithophore or diatom-
417 “dominated” community.
418 Line 676: added square brackets to “BSi” .
419 Line 683: added sentence and reference to Fig. S2, “Indeed, euphotic zone diatom
420 abundances enumerated with a FlowCam® are significantly correlated with >51
421 μm [BSi] at zPAR at corresponding stations in GB1 and GB2 (see supplement;
422 Fig. S2a).”
423 Lines 714, 726: added reference to Fig. S2 and S3.
424 Line 721: deleted “also have a short length scale of remineralization, and” .
425 Line 724: changed “the” to “a” and added “like station GB1-85” between words
426 “community” and “station GB1-25” .
427 Line 751: deleted “the remineralization length scale of calcareous assemblages is
428 likely to be longer than regions dominated by diatom assemblages” .
429
430 **5. References**
431 Line 868: capitalized second “j” in “Deep-Sea Research Part II” .
432 Line 938: deleted extra “2011” .
433 Line 960: added reference.
434 Line 1019: changed reference.
435
436 **6. Main tables and figures**
437 Table 1 caption: changed “photosynthetically active radiation” to
438 “photosynthetically available radiation” .
439 Table 2: updated error values in POC flux column. Also added footnote.
440 Table 3: updated error values in POC, PIC and BSi flux columns.
441 Fig. 2: Updated image. Also added some phrasing in caption.
442 Figs. 5-8: Added extra note about circle area in legend to end of first sentence of
443 caption for each figure.
444 Fig. 9: replaced “colorbar” with “color bar” in caption.
445 Fig. 10: replaced “colorbar” with “color bar” in caption. Also changed wording
446 in last two sentences.
447
448 **7. Supplement**
449 Table S2: Updated values in POC flux error column.
450 The table of contents, and everything after Table S2, is newly added.
451

452 Marked up changes in Main Text

453

454 **Abstract**

455

456 Sequestration of carbon by the marine biological pump depends on the processes
457 that alter, remineralize and preserve particulate organic carbon (POC) during transit to
458 the deep ocean. Here, we present data collected from the Great Calcite Belt, a calcite-rich
459 band across the Southern Ocean surface, to compare the transformation of POC in the
460 euphotic and mesopelagic zones of the water column. The ²³⁴Th-derived export fluxes
461 and size-fractionated concentrations of POC, particulate inorganic carbon (PIC), and
462 biogenic silica (BSi) were measured from the upper 1000 m of 27 stations across the
463 Atlantic and Indian sectors of the Great Calcite Belt. POC export out of the euphotic zone
464 was correlated with BSi export. PIC export was not, but did correlate positively with
465 POC flux transfer efficiency. Moreover, regions of high BSi concentrations, which
466 corresponded to regions with proportionally larger particles, exhibited higher attenuation
467 of >51 μm POC concentrations in the mesopelagic zone. The interplay among POC size
468 partitioning, mineral composition and POC attenuation suggests a more fundamental
469 driver of POC transfer through both depth regimes in the Great Calcite Belt. In particular,
470 we argue that diatom-~~rich~~ communities produce large and labile POC aggregates, which
471 generate high export fluxes but also drive more remineralization in the mesopelagic zone.
472 We observe the opposite in communities with smaller calcifying phytoplankton, such as
473 coccolithophores. We hypothesize that these differences are influenced by inherent
474 differences in the lability of POC exported by different phytoplankton communities.

475

476

477

Sarah Rosengard 5/20/15 5:49 PM

Deleted: dominated

479 **1 Introduction**

480

481 The biological pump sequesters atmospheric carbon dioxide (CO₂) in the ocean
482 (Volk and Hoffert, 1985) by way of phytoplankton-driven CO₂ fixation, followed by the
483 sinking of this fixed particulate organic carbon (POC) as aggregates and fecal pellets
484 down the water column (Riley et al., 2012). The quantity per unit area and time of POC
485 exiting the base of the euphotic zone defines the export flux, while export efficiency
486 represents the fraction of bulk primary production comprising this flux (Buesseler, 1998).

487 In the mesopelagic zone (~~from the base of the euphotic zone to ~1000 m~~), export flux
488 attenuates due to remineralization mediated by zooplankton grazing and bacteria
489 (Buesseler and Boyd, 2009; Giering et al., 2014; Martin et al., 1987). The flux of this
490 processed organic carbon leaving the mesopelagic zone, only ≤10% of export flux,
491 directly scales with the quantity of atmospheric CO₂ sequestered by the marine biological
492 pump over hundreds to thousands of years (Kwon et al., 2009).

493 On average, only ~1% of the organic matter produced by phytoplankton in the
494 surface reaches the deep sea (Martin et al., 1987). However, export and sequestration flux
495 vary widely by region, as do export efficiencies and attenuation of export flux (Buesseler
496 and Boyd, 2009; Buesseler et al., 2007; Henson et al., 2012b; Henson et al., 2011; Martin
497 et al., 1987; Thomalla et al., 2008). Such variations may drive observed differences in the
498 weight percent of organic carbon deposited at the sediment surface (Hedges and Oades,
499 1997), suggesting that the overall strength of the biological pump as a carbon sink is not
500 globally uniform. These geographical differences have spurred decades of research into
501 how mechanisms in the shallower ocean – the euphotic and mesopelagic zones – alter
502 sinking particulate organic matter during vertical transit.

503 As an example, Armstrong et al. (2002), Klaas and Archer (2002) and Francois et
504 al. (2002) posited that mineral associations with sinking organic carbon could explain
505 these variations. Their ballast hypothesis model suggested that minerals enhanced the
506 biological pump (1) by increasing the density, and consequently, the sinking speed of
507 particulate organic matter and (2) by inhibiting organic carbon remineralization down the
508 water column. Expediting vertical transit decreases the time for remineralization to act on
509 sinking particulate organic matter, increasing its chances of ~~reaching the deep sea~~. The

Sarah Rosengard 5/18/15 11:39 AM

Deleted: ~1000 m below

Sarah Rosengard 5/18/15 11:39 AM

Deleted: remaining intact on its way down

512 authors observed that calcite flux in the bathypelagic zone (>1000 m) explains roughly
513 half of the variation in the magnitude of POC flux reaching the deep sea (Klaas and
514 Archer, 2002), and may also account for some of the observed geographical variation in
515 POC flux attenuation with depth (Francois et al., 2002).

516 In its conception and infancy, the ballast hypothesis was based upon observed
517 correlations between mineral and organic carbon fluxes in the deep (>1000 m) sea. Yet,
518 evidence for the ballast mechanism in the euphotic and mesopelagic zones remains
519 equivocal, as deeper correlations are scarcely matched by shallower ocean observations
520 (Le Moigne et al., 2012). Several surface regions do not exhibit ballast correlations
521 between mineral flux and POC flux (e.g., Thomalla et al., 2008; Henson et al., 2012b). In
522 the Atlantic and Southern Oceans, Le Moigne et al. (2012) found a significant fraction of
523 POC export flux to remain unassociated with minerals altogether. Moreover, tank
524 incubations simulating POC and mineral suspensions yield conflicting results: some have
525 observed mineral associations to increase aggregate sinking rates (Engel et al., 2009),
526 while others find no such effect (Passow and De la Rocha, 2006). De La Rocha et al.
527 (2008) even suggest that sticky polymers from POC might ballast sinking minerals, rather
528 than vice-versa.

529 The scarcity of evidence supporting a shallow ocean ballast mechanism suggests
530 that the transit of particulate organic carbon in the surface, mesopelagic and deeper ocean
531 is mechanistically de-coupled (Lam et al., 2011; Lomas et al., 2010). Indeed, the debate
532 surrounding the ballast hypothesis arises from a deeper issue of whether the mechanisms
533 that influence carbon export from the euphotic zone are the same as those that control its
534 remineralization in the mesopelagic zone, and/or its transfer beyond the mesopelagic
535 zone into the deep sea.

536 The following report compares the export of organic carbon from the euphotic
537 zone with its transfer through the mesopelagic zone across the region of the Great Calcite
538 Belt (Balch et al., 2011a; Balch et al., 2014; Fig. 1). Spanning across the Southern Ocean,
539 particularly between the Subtropical and Polar Fronts, the Great Calcite Belt defines a
540 highly reflective band observed from space during each austral spring and summer. Its
541 high reflectivity is caused by calcite-rich surface waters produced by coccolithophore
542 blooms in the Southern Ocean. In this zone, coccolithophores are more abundant than in

543 regions north and south of the Belt. South of the Polar Front, coccolithophore abundances
544 decline dramatically as dissolved silica concentrations increase and diatoms flourish
545 (Balch et al., 2011a).

546 Spanning a large range in surface mineral concentrations, primary productivity,
547 and phytoplankton community composition (Balch et al., 2011a), the Great Calcite Belt
548 provides an excellent opportunity to assess the processes controlling organic carbon
549 export, export efficiency, and attenuation of POC concentration ([POC]) with depth.
550 Here, we report estimates of ^{234}Th -derived POC fluxes and [POC] through both the
551 euphotic and mesopelagic zones within the Atlantic and Indian sectors of the Great
552 Calcite Belt. We focus on the upper 1000 m of the Great Calcite Belt because the
553 attenuation of POC flux and concentration is most dramatic within this depth interval
554 (Martin et al., 1987; Lam et al., 2011). As the following discussion illuminates, this study
555 additionally weighs the ballast hypothesis against other mechanisms hypothesized to
556 control the transfer of organic carbon through the water column, and ultimately into the
557 deep sea, where carbon residence time modulates atmospheric pCO_2 and climate over
558 hundreds to thousands of years (Kwon et al., 2009).

559

560 **2 Methods**

561

562 **2.1 Field site**

563

564 Samples from the Great Calcite Belt were collected during two research cruises,
565 GB1 and GB2, which transited the Atlantic and Indian sectors of the Great Calcite Belt
566 during the austral summer of 2011 and 2012, respectively (Fig. 1), concurrent with the
567 putative coccolithophore bloom (Balch et al., 2011a). In 2011, for cruise GB1 (MV1101),
568 the *R/V Melville* crossed the Atlantic sector from Punta Arenas, Chile to Cape Town,
569 South Africa, sampling between 39°S and 59°S. One year later, for cruise GB2
570 (RR1202), the *R/V Revelle* crossed the Indian sector from Durban, South Africa to Perth,
571 Australia, sampling between 37°S and 60°S (Table 1). Both cruise tracks crossed the
572 Subtropical, Subantarctic and Polar fronts, which are approximately located at 40°S, 45°S

573 and 52°S (e.g., Belkin and Gordon, 1996; Sokolov and Rintoul, 2009), respectively,
574 defining observed shifts in temperature and nutrient characteristics of the surface ocean.

575 Each day during GB1 and GB2, 30-L Niskin samples were collected pre-dawn for
576 measuring primary production. A Biospherical Instruments (San Diego, CA) sensor was
577 mounted on the CTD/rosette and referenced to a deck sensor mounted on the ship's
578 superstructure to measure Photosynthetically Available Radiation (PAR) during the casts.
579 Water was then sampled at fixed light depths relative to surface irradiance to match light
580 levels in deck-board incubators: 36.5%, 21.1%, 11.7%, 3.55%, 1.93% and 0.28%. The
581 light depths were calculated two ways: (a) between 10:00 and 14:00 h local time (during
582 daylight hours), percentages of surface irradiance were derived directly from the
583 downcast PAR profile immediately preceding bottle firing, or (b) at all other times, the
584 light levels were back-calculated from the previously-determined relationship between
585 beam transmittance and diffuse attenuation of PAR (Balch et al., 2011b). From these
586 casts, primary production rates were measured using the ¹⁴C microdiffusion technique
587 (Paasche and Brubak, 1994) with modifications by Balch et al. (2000) (see also (Fabry
588 and Balch, 2010).

589

590 2.2 Size-fractionated particle collection

591

592 We report measurements of total and particulate ²³⁴Th activity and size-
593 fractionated particle composition from 27 stations (Fig. 1; Table 1).

594 Size-fractionated particles were collected at eight depths in the upper 1000 m of
595 fourteen stations from GB1 and thirteen stations from GB2, using modified battery
596 operated in-situ pumps (McLane WTS-LV). The modified pumps directed seawater
597 through two flow paths (Lam et al., 2014), each of which passed through a “mini-
598 MULVFS” filter holder designed to retain large particles (Bishop et al., 2012). Seawater
599 first passed through 51 µm polyester pre-filters in both filter holders for collection of
600 large (>51 µm) size-fraction particles, and then through paired 0.8 µm polyethersulfone
601 (Supor™) filters in one flow path and paired 1 µm quartz fiber (Whatman™ QMA)
602 filters in the other flow path, both of which collected small (<51 µm) size-fraction
603 particles. An average of 200 L and 500 L of seawater passed through the Supor and QMA

Sarah Rosengard 5/21/15 3:02 PM

Deleted: A

605 | flow paths over 1-2.5 hours, respectively. Immediately after collection, half to all of the
606 | >51 µm size-fraction particles from one flow path were rinsed off of the polyester pre-
607 | filters and onto 25 mm 1 µm Sterlitech silver filters using 0.2 µm-filtered seawater, and
608 | dried at 50°C for subsequent analysis of particulate ²³⁴Th, particulate organic carbon
609 | (POC), and particulate inorganic carbon (PIC, or calcium carbonate). Subsamples of
610 | QMA filters were likewise dried at 50°C for ²³⁴Th and POC analysis in the <51 µm size-
611 | fraction. Finally, the polyester pre-filters from the other flow path and Supor filters were
612 | dried in a laminar flow hood at room temperature.

613 | In the euphotic zone, where most POC is produced, these operationally defined
614 | size fractions allude primarily to the structure of phytoplankton communities producing
615 | POC (e.g., large diatoms would be found in >51 µm size-fraction particles). In the
616 | mesopelagic zone, which extends from the base of the euphotic zone to 1000 m in depth,
617 | >51 µm POC is predominantly comprised of phytoplankton and bacterial biomass that
618 | has been repackaged into aggregates and fecal pellets. The >51 µm particles collected at
619 | station GB1- 85 illustrate these different size-fraction interpretations by depth. Shallower
620 | particles collected at 25 m and 73 m, the base of the euphotic zone, are mainly comprised
621 | of intact phytoplankton cells (Figs. 2a, 2b). By contrast, deeper particles collected at 173
622 | m exhibit the features of particulate aggregates and fecal pellets (Fig. 2c).

623

624 | **2.3 Particle composition**

625

626 | Bulk concentrations of POC, PIC, biogenic silica (BSi), and particulate ²³⁴Th
627 | activity were measured in both <51 µm and >51 µm fractions of particles collected at
628 | each station. POC concentrations and ²³⁴Th activities were measured at all depths of the
629 | profiles, while [PIC] and [BSi] were mainly measured at select depths above 200 m and
630 | at the deepest depth (800-1000 m) of the profile. Particulate ²³⁴Th activities in all sub-
631 | fractions of >51 µm (25 mm silver filters) and <51 µm (25 mm QMA filters) samples
632 | were measured using low level Risø beta counters immediately on the ship and in the lab
633 | at least six ²³⁴Th half-lives post-collection for background activity.

634 | After counting for ²³⁴Th background activity, ~25% of the silver filter (~ 115 L
635 | equivalent) was fumed overnight (12-17 hours) with concentrated hydrochloric acid to

Sarah Rosengard 5/21/15 3:02 PM

Deleted: o

Sarah Rosengard 5/21/15 9:32 AM

Deleted: and depth

Sarah Rosengard 5/21/15 9:32 AM

Deleted:

639 remove inorganic carbon, before measuring >51 μm [POC] using an elemental CHN
640 analyzer. A similar protocol was followed to measure <51 μm [POC] from one 12 mm-
641 diameter subsample of each QMA filter, representing ~1% of the entire sample (~5 L
642 equivalent). Vertical profiles of >51 μm and <51 μm [POC] between the base of the
643 euphotic zone and the deepest measurement at 800 – 1000 m were fitted to a power-law
644 function to describe the attenuation of [POC] with depth, based on a function first applied
645 to POC flux by Martin et al. (1987) and then analogously to POC concentration by Lam
646 and Bishop (2007),

$$647 \quad [POC]_z = [POC]_0 \left(\frac{z}{z_{PAR}}\right)^{-b} \quad (1)$$

648 | where, at most stations, z_{PAR} represents the depth of 0.3% photosynthetically available
649 radiation (see Sect. 2.4). The exponent b represents the attenuation coefficient, with
650 higher attenuation coefficients (more negative exponents) for profiles with greater
651 attenuation of >51 μm [POC] with depth. We focus our discussion on the attenuation of
652 >51 μm [POC], because we assume that they contribute disproportionately to sinking
653 fluxes compared to the <51 μm size fraction (McCave, 1975; Lam and Bishop, 2007;
654 Lam et al., 2011). Figure 3 and Table 2 show all significant ($p < 0.05$) power law fits for
655 >51 μm [POC] profiles.

656 PIC in the samples was assumed to be biomineral calcium carbonate ($CaCO_3$),
657 and was derived from particulate calcium (Ca) corrected for salt Ca using a seawater
658 0.0382 Ca:Na (g:g) ratio (Lam and Bishop, 2007; Pilson, 2012). In the in-situ pump
659 samples, salt-derived Ca typically accounted for ~60% of total Ca. The >51 μm PIC size-
660 fraction concentrations were measured mainly in subsamples of remaining pre-filter
661 material and occasionally in sub-fractions of the silver filters, if the former were
662 unavailable. The <51 μm size fraction [PIC] was measured in three 12mm circular QMA
663 subsamples, representing ~15 L or ~3% of the sample. Subsamples were leached in 0.6 N
664 ultrapure Sea-Star™ Baseline hydrochloric acid (HCl) at 60°C for 12-16 hours. The
665 leachate was subsequently filtered through a 0.4 μm polycarbonate membrane filter,
666 diluted to 0.12 N HCl, and spiked with 1 ppb of Indium as an internal standard. The
667 spiked leachate solution was then analyzed for Ca, Na and P using an Element 2 sector-
668 field inductively-coupled plasma mass spectrometer (ICP-MS) in medium and high

Sarah Rosengard 5/18/15 10:41 PM

Deleted: below

Sarah Rosengard 5/20/15 3:01 PM

Deleted: active

671 resolution. Counts per second were converted to concentration using external mixed
672 element standard curves.

673 For measuring $>51 \mu\text{m}$ and $<51 \mu\text{m}$ [BSi], prefilter or Supor subsamples,
674 respectively, were leached in 0.2 N sodium hydroxide at 85°C for one hour, and analyzed
675 by standard spectrophotometric detection of the blue silico-molybdate complex in each
676 leachate within 24 hours of the leach (Strickland and Parsons, 1968; Brzezinski and
677 Nelson, 1989). Absorbance through each sample was converted to concentration using an
678 external Si standard curve.

679

680 2.4 ^{234}Th -derived flux estimates

681

682 Particle fluxes were estimated at each station by measuring the water-column
683 disequilibrium between ^{234}Th and ^{238}U in the upper 350 m of the water-column (Savoye
684 et al., 2006). ^{234}Th is the radioactive daughter of ^{238}U with a short enough half-life (24.1
685 days) relative to ^{238}U such that it is assumed to be in secular equilibrium with its parent
686 isotope in the absence of particle scavenging (i.e., ^{234}Th activity = ^{238}U activity).

687 Disequilibria between the two isotope activities in the water column are attributed to the
688 scavenging of ^{234}Th by sinking particles (Savoye et al., 2006). Integrating the deficit in
689 ^{234}Th relative to ^{238}U provides a measure of particle flux down the water column
690 (Buesseler et al., 2006). Because of the short half-life of ^{234}Th , deviation from secular
691 equilibrium exists only in regions of high particle flux. Thus, ^{234}Th -based flux estimates
692 are most frequently applied in the euphotic zone of the ocean where particle export is
693 maximal.

694 ^{234}Th - ^{238}U deficits were determined by measuring total water-column activities of
695 both isotopes. ^{238}U activity ($A_{\text{U-238}}$) profiles were calculated from salinity by the
696 following relationship (Owens et al., 2011):

$$697 \quad A_{\text{U-238}} \left(\frac{\text{dpm}}{\text{L}} \right) = (0.0786 \times \text{Salinity}) - 0.315 \quad (2)$$

698 Total water-column ^{234}Th activity ($A_{\text{Th-234}}$) profiles were determined from 4 L seawater
699 samples collected by CTD casts down to 300-350 m at each station (Pike et al., 2005).

700 Shortly after collection, each 4 L seawater sample was acidified to pH 2 using
701 concentrated nitric acid (HNO_3), spiked with 1 g of ^{230}Th of a known activity (50.06 dpm

702 g^{-1}) as a yield monitor, equilibrated for 8 hours, and finally brought up to pH 8.5 using
 703 ammonium hydroxide (NH_4OH) (van der Loeff et al., 2006). Manganese chloride
 704 (MnCl_2) and potassium permanganate (KMnO_4) were added to the neutralized seawater
 705 to form a manganese oxide (MnO_2) precipitate, which efficiently scavenges both natural
 706 ^{234}Th and added ^{230}Th . After 12 hours, the precipitate was filtered onto a quartz fiber
 707 filter, dried at 50°C , and then mounted beneath a sheet of Mylar and aluminum foil. ^{234}Th
 708 activity in the precipitate was measured on board by low level Risø beta counters and
 709 post-cruise after at least six ^{234}Th half-lives for background activity. The ^{230}Th spike was
 710 recovered by fully dissolving the MnO_2 precipitate, adding a 1 g spike of ^{229}Th of a
 711 known activity (69.74 dpm g^{-1}), and measuring $^{229}\text{Th}:$ ^{230}Th ratios on an Element 2 sector-
 712 field ICP-MS in low resolution. Recovery of ^{230}Th spike was derived from this ratio, and
 713 used to correct for inefficiencies in the scavenging of total seawater ^{234}Th by MnO_2
 714 precipitation.

715 To calibrate beta counting efficiency for each cruise, total deep water (i.e., below
 716 2000 m) ^{234}Th activities were compared to total deep water ^{238}U activities, as measured in
 717 4-5 replicate samples from 2-3 deep water CTD casts during each cruise (at 5000 m
 718 during GB1, and at 2500 m during GB2). Beta counting efficiencies were adjusted such
 719 that ^{234}Th and ^{238}U activities were equal in these deep measurements, as secular
 720 equilibrium would be expected at such depths. We only report upper water-column
 721 activities (<350 m) after correcting for experimental efficiencies in both the seawater
 722 collection process and beta detector counting. Uncertainties in the total ^{234}Th activity
 723 profiles averaged 4.5% and were propagated from errors associated with counting
 724 statistics, recoveries, and beta-counting efficiency.

725 To calculate ^{234}Th export flux, ^{234}Th activity deficits were integrated down to the
 726 base of the euphotic zone (z_{PAR}) (Buesseler et al., 2008; Thomalla et al., 2008):

$$727 \quad ^{234}\text{Th Flux} \left(\frac{\text{dpm}}{\text{m}^2\text{d}} \right) = \int_0^{z_{\text{PAR}}} (A_{\text{U-238}} - A_{\text{Th-234}}) dz \quad (3)$$

728 At most stations, the export depth, z_{PAR} , was chosen to be the depth where light
 729 levels were 0.3% of surface-level PAR. The exception was station GB2-27, which did not
 730 include a PAR measurement profile. For this station, the z_{PAR} value of 105 m was defined
 731 as the depth where the transmissometry-based particle concentration decreased. These
 732 export depths were compared to one additional metric describing particle concentration in

733 seawater: the depths where ^{234}Th and ^{238}U activities re-established secular equilibrium, or
734 $z_{\text{Th/U}}$. We explore the sensitivity of ^{234}Th flux estimates to choice of z_{PAR} in Sects. 3 and
735 4.1.

736 ^{234}Th flux estimates were converted to POC, PIC and BSi fluxes by multiplication
737 with ratios of $>51\ \mu\text{m}$ POC, PIC, and BSi concentrations to particulate ^{234}Th activity in
738 samples at z_{PAR} (Thomalla et al., 2008; Sanders et al., 2010):

$$739 \quad \text{POC Flux} \left(\frac{\mu\text{mol}}{\text{m}^2\text{d}} \right) = [\text{POC}] : A_{\text{Th}-234} \times ^{234}\text{Th Flux} \left(\frac{\text{dpm}}{\text{m}^2\text{d}} \right) \quad (4)$$

$$740 \quad \text{PIC Flux} \left(\frac{\mu\text{mol}}{\text{m}^2\text{d}} \right) = [\text{PIC}] : A_{\text{Th}-234} \times ^{234}\text{Th Flux} \left(\frac{\text{dpm}}{\text{m}^2\text{d}} \right) \quad (5)$$

$$741 \quad \text{Si Flux} \left(\frac{\mu\text{mol}}{\text{m}^2\text{d}} \right) = [\text{BSi}] : A_{\text{Th}-234} \times ^{234}\text{Th Flux} \left(\frac{\text{dpm}}{\text{m}^2\text{d}} \right) \quad (6)$$

742

743 **2.5 Interpolation of data**

744

745 In all cases where ^{234}Th activity, $>51\ \mu\text{m}$ and $<51\ \mu\text{m}$ [POC] and mineral
746 concentrations, and $>51\ \mu\text{m}$ particulate ^{234}Th measurements were unavailable at z_{PAR} ,
747 linear interpolations between the sampling depths above and below z_{PAR} were used to
748 estimate a value at the export depth (Table 1). The $>51\ \mu\text{m}$ and $<51\ \mu\text{m}$ size-fraction
749 POC concentrations were interpolated by the power law attenuation function when fits
750 were significant ($p < 0.05$), or linearly when these power-law fits were not significant or
751 inconsistent with the broader shape of the [POC] profile at that particular station. In
752 general, corresponding POC: ^{234}Th , BSi: ^{234}Th , and PIC: ^{234}Th ratios are quotients of these
753 interpolated values except as noted in Tables 2 and 3.

754

755 **3 Results**

756

757 ^{234}Th activity profiles were measured over the upper 300 – 350 m at the 27
758 stations of cruises GB1 and GB2 (Fig. 4; Table S1). Each activity profile is associated
759 with two metrics that have been used in previous studies to define the export depth (see
760 Sect. 2.4): the base of the euphotic zone (z_{PAR}), which we define at 0.3% surface
761 photosynthetically available radiation (PAR) (e.g., Buesseler and Boyd 2009), and $z_{\text{Th/U}}$,
762 where ^{234}Th and ^{238}U activities re-establish secular equilibrium (Table 1). In most

763 stations, profiles exhibited ^{234}Th activity deficits over a range from surface to 75 – 170 m
764 in depth, below which ^{234}Th activity generally returned to secular equilibrium with ^{238}U
765 activity, within error. The notable exceptions were profiles at stations GB1-6, and GB1-
766 16, which did not return to secular equilibrium by 170 m in depth. Considering that
767 stations GB1-6 and GB1-16 are closest to shore, their sustained ^{234}Th deficits may have
768 been influenced by lateral advection of particles from the continental shelf. At these
769 stations, $z_{\text{Th/U}}$ depths were approximated by the depth below which ^{234}Th activities remain
770 constant with depth. For example, at station GB1-6, $z_{\text{Th/U}} = 130$ m because below this
771 depth ^{234}Th activities remained relatively constant.

772 In the Atlantic sector, sampled in January – February 2011, all observed z_{PAR}
773 depths were significantly shallower than $z_{\text{Th/U}}$ depths (Student's t-test $p < 0.05$); on
774 average, z_{PAR} was 66 ± 44 % shallower than $z_{\text{Th/U}}$. By contrast, in the Indian sector,
775 sampled roughly a year later in February – March 2012, z_{PAR} was not significantly
776 different from $z_{\text{Th/U}}$ ($p > 0.05$), and the average relative difference was -6 ± 29 %. In
777 general, when water-column ^{234}Th activity is at steady-state, the euphotic zone should
778 correspond to the region of ^{234}Th deficit relative to ^{238}U (Buesseler et al., 2008; Buesseler
779 and Boyd, 2009), i.e., z_{PAR} should equal $z_{\text{Th/U}}$.

780 Using integrated activity deficits, export fluxes of ^{234}Th , POC, PIC, and BSi at
781 z_{PAR} were estimated at the 27 sites (Figs. 5, 6; Table 3). Overall mean ^{234}Th fluxes at z_{PAR}
782 were $1,413 \pm 432$ dpm $\text{m}^{-2} \text{d}^{-1}$ (mean ± 1 s.d.), and ranged from 717 to 2,437 dpm $\text{m}^{-2} \text{d}^{-1}$
783 at stations GB2-112 and GB1-6, respectively. Mean derived POC fluxes at z_{PAR} were 4.5
784 ± 3.9 mmol $\text{m}^{-2} \text{d}^{-1}$, ranging from 0.97 to 20 mmol $\text{m}^{-2} \text{d}^{-1}$ at stations GB2-112 and GB1-
785 85, respectively. Mean PIC fluxes were 1.2 ± 1.7 mmol $\text{m}^{-2} \text{d}^{-1}$, and ranged from 0.067 to
786 6.2 mmol $\text{m}^{-2} \text{d}^{-1}$ at stations GB2-73 and GB1-59, respectively. Finally, mean BSi fluxes
787 at z_{PAR} were 3.8 ± 5.8 mmol $\text{m}^{-2} \text{d}^{-1}$, ranging from 0.17 to 28 mmol $\text{m}^{-2} \text{d}^{-1}$ at stations
788 GB2-46 and GB1-85, respectively. Higher POC export stations frequently corresponded
789 with higher BSi export stations (e.g., station GB1-85), but less so with higher PIC export
790 stations.

791 The highest and lowest measured biomineral (PIC and BSi) fluxes at z_{PAR} were in
792 GB1 and GB2, respectively, but mean values were not significantly different between
793 ocean basins because of high variability within each basin (Fig. 6). However, mean POC

794 fluxes at z_{PAR} were significantly higher in GB1 (mean \pm 1 s.d.= 6.0 ± 4.9 mmol $m^{-2} d^{-1}$)
795 than in GB2 (3.0 ± 1.7 mmol $m^{-2} d^{-1}$) (Student's t-test $p > 0.05$). Because POC: ^{234}Th values
796 did not differ between GB1 and GB2 ($p < 0.05$), we attribute this inter-basin difference in
797 POC fluxes primarily to significantly higher ^{234}Th fluxes in GB1 ($1,574 \pm 463$ dpm $m^{-2} d^{-1}$)
798 relative to fluxes in GB2 ($1,240 \pm 330$ dpm $m^{-2} d^{-1}$).

799 Further, there were significant latitudinal differences among export fluxes and
800 particulate composition ratios in three temperature/nutrient regimes across both sectors
801 (Fig. 1; Table 4): (1) north of $45^\circ S$, the approximate location of the Subantarctic front,
802 where temperatures exceeded $\sim 10^\circ C$; (2) south of $52^\circ S$, the approximate location of the
803 Polar Front (e.g., Belkin and Gordon, 1996; Sokolov and Rintoul, 2009), where
804 temperatures remained below $\sim 5^\circ C$; and (3) between $45^\circ S$ and $52^\circ S$, where
805 temperatures ranged from ~ 5 - $10^\circ C$. The $> 51 \mu m$ size-fraction POC: ^{234}Th values at z_{PAR}
806 were significantly lower in the most equatorward zone north of $45^\circ S$, where average
807 ratios were $1.9 \pm 0.9 \mu mol dpm^{-1}$. The highest average ratios, south of $52^\circ S$, were $5.4 \pm$
808 $3.0 \mu mol dpm^{-1}$, illustrating the wide variation in POC: ^{234}Th ratios with ecosystem type
809 (Buesseler et al., 2006; Jacquet et al., 2011). Likewise, zonally averaged POC export
810 fluxes in the most equatorward zone (2.7 ± 2.3 mmol $m^{-2} d^{-1}$) were significantly lower
811 than average fluxes in the most poleward zone (8.0 ± 6.3 mmol $m^{-2} d^{-1}$). BSi: ^{234}Th values
812 were significantly different in all three zones, with highest average ratios south of $52^\circ S$
813 ($7.1 \pm 4.1 \mu mol dpm^{-1}$) and smallest ratios north of $45^\circ S$ ($0.3 \pm 0.1 \mu mol dpm^{-1}$).
814 Similarly, average BSi export fluxes were also significantly different from each other in
815 all three zones, with the greatest average values south of $52^\circ S$ (10 ± 8.7 mmol $m^{-2} d^{-1}$),
816 and lowest values north of $45^\circ S$ (0.35 ± 0.16 mmol $m^{-2} d^{-1}$). Finally, PIC: ^{234}Th ratios,
817 which averaged $0.72 \pm 0.85 \mu mol dpm^{-1}$ across all zones, and PIC export fluxes were not
818 significantly different from each other in any zone defined by these latitudinal bands.

819 These fluxes are sensitive to the choice of export depth (z_{PAR} or $z_{Th/U}$), not only
820 because the export depth determines the magnitude of ^{234}Th flux by influencing the
821 integrated ^{234}Th deficit, but also because the export depth determines which POC: ^{234}Th
822 ratio best describes particles sinking from the chosen depth (Fig. S1). Across stations, the
823 depth metrics z_{PAR} and $z_{Th/U}$ differed from each other to varying extents (Fig. 4; Table 1).
824 As exemplified by stations GB1-92, GB1-16, and GB2-100, POC fluxes changed

825 significantly between z_{PAR} and $z_{Th/U}$ (Figs. 5b, 5c; Table S2). At station GB1-92, where
826 z_{PAR} was 40 m shallower than $z_{Th/U}$, POC flux decreased from $8.0 \text{ mmol m}^{-2} \text{ d}^{-1}$ at z_{PAR} to
827 $5.1 \text{ mmol m}^{-2} \text{ d}^{-1}$ at $z_{Th/U}$. In contrast, at station GB1-16, where z_{PAR} was 80 m shallower
828 than $z_{Th/U}$, POC fluxes increased from $5.9 \text{ mmol m}^{-2} \text{ d}^{-1}$ to $6.6 \text{ mmol m}^{-2} \text{ d}^{-1}$. At station
829 GB2-100, one of few stations where z_{PAR} was deeper than $z_{Th/U}$, POC fluxes decreased
830 from 3.3 to $1.5 \text{ mmol m}^{-2} \text{ d}^{-1}$ going deeper. At this station, the POC: ^{234}Th ratio at $z_{Th/U}$
831 was 102% greater than ratios at z_{PAR} , while ^{234}Th fluxes at $z_{Th/U}$ were 6% greater than
832 fluxes at z_{PAR} , demonstrating that changes in particle composition disproportionately
833 contributed to the observed difference in POC export at z_{PAR} and $z_{Th/U}$. By contrast, at
834 station GB1-16, the relative change in ^{234}Th fluxes from z_{PAR} to $z_{Th/U}$ (+29%) contributed
835 more to the increase in POC flux with depth than the relative change in POC: ^{234}Th ratio
836 (-13%). Finally, for station GB1-92, the relative change in ^{234}Th flux with depth (-19%)
837 was similar to the relative change in POC: ^{234}Th with depth (-21%), demonstrating that
838 the export flux estimate was equally sensitive to changes in both parameters.

839

840 **4 Discussion**

841

842 The following discusses these flux measurements in the context of other Southern
843 Ocean observations, and hypotheses surrounding the transformation of sinking organic
844 carbon within the euphotic and mesopelagic zones of the water column.

845

846 **4.1 Choice of export depth**

847

848 The two possible depths we use to calculate export flux, z_{PAR} and $z_{Th/U}$, are
849 significantly different in the Atlantic sector, which influences the magnitude of flux
850 estimated (see Sect. 3). We offer here two possible and not mutually exclusive
851 explanations for why $z_{Th/U}$ depths were on average deeper than z_{PAR} depths at GB1
852 stations.

853 One hypothesis is that the ^{234}Th - ^{238}U profiles used to calculate export fluxes may
854 not have been at steady-state during the time of sampling on the GB1 cruise. Non-steady
855 state conditions in the ^{238}U - ^{234}Th system do occur during phytoplankton blooms,

856 particularly during their decline and ascent (Savoie et al., 2006; Buesseler et al., 2009).
857 For example, a recent and rapid increase in the near-surface particle concentration could
858 decrease the depth of light penetration faster than the ^{238}U - ^{234}Th system can adjust,
859 leading to a z_{PAR} measured on station that is shallower than the $z_{\text{Th/U}}$, which reflects
860 conditions prior to the rapid increase. Since the GB1 cruise in the Atlantic sector took
861 place a month earlier in the growing season (January-February 2011) than the GB2 cruise
862 in the Indian sector (February-March 2012), the two sectors may have been sampled at
863 different stages of the seasonal bloom, contributing to differences in agreement between
864 z_{PAR} and $z_{\text{Th/U}}$. Satellite chlorophyll time-series, if well-resolved, can shed light on how
865 dynamic primary production was around the time of sampling at each station of GB1 and
866 GB2, whether rapid (i.e., within three weeks) changes in particle production and sinking
867 fluxes from a bloom could have decoupled ^{234}Th - ^{238}U deficits from light profiles into the
868 surface ocean of the Great Calcite Belt. Eight-day composites of chlorophyll imagery
869 from December 2010 to February 2011 were required to overcome spatial patchiness in
870 the data due to clouds, and indicate that the changes leading up to sampling during GB1
871 were not consistent across all stations where $z_{\text{PAR}} < z_{\text{Th/U}}$. At several stations, chlorophyll
872 concentrations declined towards the sampling date; at others, chlorophyll did not change
873 or increased towards the sampling date. Moreover, out of the three stations where $z_{\text{PAR}} =$
874 $z_{\text{Th/U}}$, only one exhibited relatively constant chlorophyll concentrations in the month
875 preceding sampling. In GB2, where the differences between z_{PAR} and $z_{\text{Th/U}}$ were not
876 significant, chlorophyll tended to be constant preceding more sampling stations.
877 Nonetheless, as in GB1, several locations still experienced increasing or decreasing
878 chlorophyll concentrations in the weeks before sampling, despite having a similar z_{PAR}
879 and $z_{\text{Th/U}}$.

880 The inability of the chlorophyll time-series to unequivocally resolve the
881 differences between z_{PAR} and $z_{\text{Th/U}}$ points to other possible mechanisms underlying the
882 discrepancy. One other mechanism, which does not necessarily preclude non-steady state
883 in the ^{234}Th system, is sinking particle production below the euphotic zone z_{PAR} (Trull et
884 al., 2008). Physical aggregation and fecal pellet production by zooplankton grazing in the
885 region below z_{PAR} (i.e., the upper mesopelagic zone) can increase the speed and total
886 abundance of sinking of particles by transforming phytoplankton biomass exiting the

Sarah Rosengard 5/21/15 9:36 AM

Deleted: productivity

Sarah Rosengard 5/21/15 9:36 AM

Deleted: productivity

Sarah Rosengard 5/18/15 2:02 PM

Deleted: experienced

Sarah Rosengard 5/18/15 2:02 PM

Deleted: primary productivity

Sarah Rosengard 5/21/15 9:37 AM

Deleted: primary productivity

Sarah Rosengard 5/21/15 9:37 AM

Deleted: productivity

893 euphotic zone, thereby contributing to sustained ^{234}Th deficits below z_{PAR} (Steinberg et
894 al., 2008; Wilson et al., 2008; Abramson et al., 2010). Why this occurs only in GB1 and
895 not GB2 is not known.

896 For example, the ~70m difference in z_{PAR} and $z_{\text{Th/U}}$ at a station like GB1-85
897 (Table 1) may be attributed to additional production or repackaging of sinking particles in
898 the upper mesopelagic zone, causing ^{234}Th deficits to persist beyond the euphotic zone of
899 primary productivity, and a deeper $z_{\text{Th/U}}$. Images of >51 μm particles from this station
900 highlight the changing nature of >51 μm particles with depth (Fig. 2), from primarily
901 large phytoplankton in the euphotic zone to predominantly fecal pellets in the
902 mesopelagic zone. The difference in POC fluxes measured at both depths may arise from
903 the evolution of these particles during vertical transit, from predominantly intact and
904 relative buoyant diatoms at z_{PAR} to degraded, sinking fecal pellets produced between z_{PAR}
905 and $z_{\text{Th/U}}$.

906 Going forward, it is most important to keep in mind how the choice of export
907 depth impacts flux estimates. For this study, all export fluxes are defined by z_{PAR} so that
908 they can be compared with integrated primary production measurements (Buesseler and
909 Boyd, 2009). Non-steady-state effects of ^{234}Th profiles on export fluxes will not be
910 considered further because we do not have Lagrangian observations at multiple time
911 points necessary to detect such effects (Buesseler et al., 2003; Resplandy et al., 2012).

912

913 4.2 Comparison of export fluxes to previous studies

914

915 The ^{234}Th fluxes we report (mean \pm S.D. = $1,413 \pm 432 \text{ dpm m}^{-2} \text{ d}^{-1}$) are generally
916 within range of measurements from other Southern Ocean studies ($1,615 \pm 1,050 \text{ dpm m}^{-2}$
917 d^{-1}) (compilation by Le Moigne et al., 2013; Shimmield et al., 1995; Rutgers Van Der
918 Loeff et al., 1997; Buesseler, 1998; Cochran et al., 2000; Buesseler et al., 2001; Friedrich
919 and van der Loeff, 2002; Buesseler et al., 2003; Coppola et al., 2005; Morris et al., 2007;
920 Thomalla et al., 2008; Savoye et al., 2008; Rodriguez y Baena et al., 2008; Jacquet et al.,
921 2011; Rutgers van der Loeff et al., 2011; Zhou et al., 2012; Planchon et al., 2013). By
922 contrast, the POC fluxes we report ($4.5 \pm 3.9 \text{ mmol m}^{-2} \text{ d}^{-1}$) are on average three times
923 lower than fluxes from other studies ($12.6 \pm 13.3 \text{ mmol m}^{-2} \text{ d}^{-1}$) due to lower POC. ^{234}Th

Sarah Rosengard 5/19/15 12:09 PM

Deleted: e.g.,

Sarah Rosengard 5/19/15 12:01 PM

Deleted: (

Sarah Rosengard 5/19/15 12:09 PM

Deleted: ;

Sarah Rosengard 5/19/15 12:02 PM

Formatted: Superscript

927 ratios measured in $>51 \mu\text{m}$ particles. In general, POC: ^{234}Th ratios can vary widely as a
928 function of season, ecosystem composition, size-fraction, depth, and particle sampling
929 methodology (Coppola et al., 2005; Buesseler et al., 2006; Santschi et al., 2006; Jacquet
930 et al., 2011). In GB1 and GB2, an ecosystem effect likely accounts for the 14-fold
931 difference in POC: ^{234}Th between oligotrophic waters (e.g. $0.8 \mu\text{mol dpm}^{-1}$ at GB2-106)
932 and polar waters (e.g., $10.8 \mu\text{mol dpm}^{-1}$ at GB1-85) (Table 3). The Le Moigne et al.
933 (2013) dataset may include more studies from diatom-rich ecosystems with high
934 POC: ^{234}Th organic particles, such as observed by Buesseler (1998; not included in Le
935 Moigne et al. 2013), driving some of the discrepancy between our observations and POC
936 fluxes reported by (Le Moigne et al., 2012).

937 Other potential reasons for POC: ^{234}Th differences are the choice of export depth
938 (see Sect. 4.1) and different sampling methodologies in the previous studies. For instance,
939 in-situ pump filter holders with a small-diameter central intake and thus higher intake
940 velocities have been observed to sample more zooplankton, which typically have higher
941 POC: ^{234}Th ratios, than filter holders with diffuse intakes (Bishop et al., 2012). This is
942 because swimming zooplankton can avoid the gentle intake velocities of filter holders
943 with diffuse intakes but not the higher velocities of small diameter intakes. This would
944 be expected to affect estimates of ^{234}Th -derived POC flux more than ^{234}Th -derived
945 biomineral fluxes.

946 There have been far fewer estimates of ^{234}Th -derived biomineral export fluxes
947 (Thomalla et al., 2008; Sanders et al., 2010; Le Moigne et al., 2012; Le Moigne et al.,
948 2013). BSi and PIC fluxes observed during GB1 and GB2 are within the range
949 previously observed during the *Crozex* study by the Crozet islands (Le Moigne et al.,
950 2012), the site of station GB2-27. Thomalla et al. (2008) also reported biomineral fluxes
951 from the Atlantic Meridional Transect (AMT), north of the Subantarctic Front. While
952 AMT PIC export fluxes were only two times smaller than our mean PIC fluxes in the
953 Great Calcite Belt region, AMT BSi fluxes were ten times smaller. The disparity in BSi
954 fluxes is unsurprising, since the AMT cruise track was through waters with low
955 abundance of silicifiers. We also find that the PIC and BSi fluxes from our Great Calcite
956 Belt study are 4 and 10 times larger than biomineral fluxes estimated by Henson et al.
957 (2012b), respectively, who used a steady-state model of nutrient uptake against nutrient

958 export (Sarmiento et al., 2002; Sarmiento et al., 2004). The Henson et al. method used
959 annual climatologies of nutrient concentration profiles for their estimates, whereas the
960 ²³⁴Th-derived export method used here integrates over several weeks in the growing
961 season. This difference in timescales of integration likely accounts for the smaller
962 biomineral fluxes in Henson et al. (2012b).

963

964 **4.3 Export efficiency**

965

966 We found no significant relationship observed between integrated primary
967 productivity and POC flux at z_{PAR} , highlighting the variable export efficiency across GB1
968 and GB2. Export efficiencies, or “EZ-ratios” (Buesseler and Boyd, 2009), were calculated
969 as the ratio of POC flux at z_{PAR} to total integrated primary production in the euphotic
970 zone (Fig. 7b; Table 3). Mean export efficiencies were 0.26 ± 0.19 , and ranged from 0.04
971 to 0.77 at stations GB1-16 and GB2-63, respectively. The lack of association between
972 primary productivity and POC export flux confirms previously observed decoupling
973 between the factors that drive export and those that modulate primary productivity
974 (Buesseler et al., 2001; Coppola et al., 2005; Maiti et al., 2012).

975

976 **4.4 Vertical attenuation of POC flux and concentration**

977

978 At most stations, both POC flux and $>51 \mu\text{m}$ [POC] decline with depth below
979 z_{PAR} as a result of remineralization. In the following, we use two metrics to describe POC
980 transfer in the mesopelagic zone: (1) the attenuation of $>51 \mu\text{m}$ [POC] in the mesopelagic
981 zone, expressed as the attenuation coefficients extracted from power-law fits of
982 mesopelagic $>51 \mu\text{m}$ [POC] (exponent from Eq. (1)) and (2) the POC flux transfer
983 efficiency (T_{100}), defined as the fraction of ²³⁴Th-based POC flux that survives
984 remineralization and is transferred 100 m below z_{PAR} (Buesseler and Boyd, 2009). The
985 first metric describes the disappearance of POC concentration, and applies to the entire
986 mesopelagic zone; the second metric describes the survival of POC flux, and applies to
987 the upper mesopelagic zone.

Sarah Rosengard 5/18/15 3:32 PM

Deleted: 2010

989 The mean T_{100} was 0.71 ± 0.38 , ranging from 0.20 to 1.8 at stations GB2-119 and
990 GB1-25, respectively (Fig. 7c; Table 2), generally falling within the spread of values
991 observed globally as well as specifically in the Southern Ocean (Buesseler and Boyd,
992 2009). At stations GB1-6, GB1-16, GB1-25, GB1-59, and GB2-106, T_{100} values are
993 greater than 1.0 and reflect an increase in POC flux with depth between z_{PAR} and 100_m
994 below z_{PAR} (Figs. 5b, 5d). Transfer efficiencies greater than 1 can occur during a
995 declining bloom (Henson et al., 2015), but examination of satellite chlorophyll time-
996 series does not indicate that these stations were sampled at such conditions. At GB1-6,
997 GB1-16 and GB1-59, the ^{234}Th - ^{238}U disequilibrium extends relatively deep (>200m) into
998 the water column, thus leading to continually increasing ^{234}Th flux with depth, suggesting
999 that either renewed particle production at depth or lateral advection of particles away
1000 from these coastal stations could sustain the ^{234}Th deficit below z_{PAR} . Moreover, because
1001 z_{PAR} depths are significantly shallower than $z_{Th/U}$ in most GB1 stations, including GB1-6,
1002 GB1-16 and GB1-59, the transfer efficiency calculation at these stations in GB1 captures
1003 an increase in ^{234}Th flux between z_{PAR} and 100 m below z_{PAR} . Thus, for the following
1004 discussion, it is important to view transfer efficiency values with the caveat that GB1 and
1005 GB2 stations display different ^{234}Th - ^{238}U disequilibria profiles with respect to z_{PAR} and
1006 $z_{Th/U}$, and this difference impacts all calculations that use a ^{234}Th flux component.

1007 At the two other stations for which $T_{100} > 1$, GB1-25 and GB2-106, the increases in
1008 POC flux below z_{PAR} arise primarily from increasing POC: ^{234}Th ratios rather than
1009 increasing ^{234}Th flux with depth (Figs. S1a, S1d). The increase in these ratios results from
1010 a faster decrease in particulate ^{234}Th activity compared to changes in $>51 \mu m$ [POC] with
1011 depth. This is unexpected and at all other stations, $>51 \mu m$ [POC] decreases more quickly
1012 than particulate ^{234}Th activity due to organic carbon remineralization. We suspect that
1013 poor $>51 \mu m$ particle distribution on filters from GB2-106 may have led to anomalously
1014 low POC around z_{PAR} , but do not have an explanation for the consistent increase in
1015 POC:Th with depth at GB1-25 (Figs. S1a). We proceed by excluding the T_{100} transfer
1016 efficiencies from these two stations from statistical tests, but identify them for
1017 completeness (Figs. 7, 9).

1018 The general decline in POC flux with depth at most stations is mirrored by a
1019 decrease in $>51 \mu m$ [POC], both of which are a result of remineralization. Attenuation

Sarah Rosengard 5/18/15 5:46 PM

Deleted: where

Sarah Rosengard 5/21/15 9:41 AM

Deleted: a sampling issue and thus exclude

Sarah Rosengard 5/21/15 9:41 AM

Deleted: further consideration

1023 coefficients from power-law fits of mesopelagic $>51 \mu\text{m}$ [POC] at 22 stations describe
1024 this transformation from z_{PAR} to the lower mesopelagic zone, where $>51 \mu\text{m}$ [POC]
1025 between 800-1000 m was 1.5 to 137 times lower than $>51 \mu\text{m}$ [POC] at z_{PAR} (Figs. 8b,
1026 8c; Table 2). We discount the attenuation value at station GB2-93 from discussion
1027 because it had an anomalously low $>51 \mu\text{m}$ [POC] at 800m, likely due to incomplete
1028 rinsing of particles from the prefilter. This drove the power law fit to yield an
1029 anomalously high attenuation coefficient, an outlier, as approximated by Chauvenet's
1030 Theorem (Glover et al., 2011). Attenuation coefficients were 1.1 ± 0.50 on average, and
1031 varied from 0.4 to 1.9 at stations GB1-25 and GB2-43, respectively (Fig. 8c; Table 2),
1032 which spans the global range compiled by Lam et al. (2011).

1033 The $>51 \mu\text{m}$ [POC] at z_{PAR} is not correlated with $>51 \mu\text{m}$ [POC] at lower
1034 mesopelagic depths, suggesting that processes controlling $>51 \mu\text{m}$ [POC] at the top of the
1035 mesopelagic differ from those controlling $>51 \mu\text{m}$ [POC] at the base of the mesopelagic
1036 zone. This is supported by the great variation in attenuation coefficients and transfer
1037 efficiencies, and suggests that POC concentrations at z_{PAR} are decoupled from [POC] at z
1038 $\geq 800\text{m}$, as has also been noted in other POC flux and concentration observations (Lomas
1039 et al., 2010; Lam et al., 2011; Henson et al., 2012b). There are some exceptions, such as
1040 at GB1-85, which exhibited the highest $>51 \mu\text{m}$ [POC] both at z_{PAR} and below 800 m, but
1041 there is no overall relationship across the dataset. The remaining discussion aims to tease
1042 apart the processes that control POC flux and $>51 \mu\text{m}$ [POC] in each depth regime.

1043

1044 **4.5 Biomineral-POC flux correlations at z_{PAR}**

1045

1046 We compared POC fluxes to mineral fluxes at z_{PAR} (Figs. 9a, 9b) to test the
1047 hypothesis that mineral ballasting facilitates POC export out of the euphotic zone, as has
1048 been observed in deeper flux datasets $>1000 \text{ m}$ (Klaas and Archer, 2002; Armstrong et
1049 al., 2002; Francois et al., 2002). Because we use ^{234}Th activity deficits and the same
1050 particulate ^{234}Th activities to derive all fluxes (Eq. (4-6)), comparing export fluxes is
1051 equivalent to comparing concentrations of $>51 \mu\text{m}$ POC, BSi and PIC at z_{PAR} . In this
1052 dataset, minor differences between flux versus concentration comparisons (not shown)

1053 arise from differences in interpolation methods for POC:²³⁴Th, BSi:²³⁴Th, and PIC:²³⁴Th
1054 ratios at Z_{PAR} (Table 3).

1055 Pearson correlation tests between shallow POC export and the two biomineral
1056 fluxes revealed a significantly positive correlation between POC and BSi fluxes
1057 ($p \ll 0.001$, $r^2 = 0.77$). By contrast, there was no significant relationship between shallow
1058 POC and PIC fluxes ($p = 0.24$, $r^2 = 0.06$). Both BSi and POC export fluxes tend to increase
1059 poleward from the region north of the Subtropical/Subantarctic fronts to the inter-frontal
1060 zone to the region south of the Polar front (Figs. 5b, 6a, 6b). Station GB1-85, which sits
1061 just south of the Polar Front ($\sim 52^\circ\text{S}$), is a high BSi and POC flux outlier. When removed,
1062 the BSi flux vs. POC flux correlation remains significant, though weaker ($r^2 = 0.43$),
1063 suggesting that although this correlation is strongly influenced by station GB1-85, the
1064 shallow BSi ballast association still remains valid for the rest of the dataset.

1065 We also compared POC export fluxes to both PIC and BSi export fluxes
1066 simultaneously by multiple linear regression:

1067
$$\text{POC Flux} = (m_{\text{BSi}} \times \text{BSi Flux}) + (m_{\text{PIC}} \times \text{PIC Flux}) + \text{constant} \quad (7)$$

1068 The multiple linear regression only explains an additional 5% of the variance in POC flux
1069 at Z_{PAR} ($r^2 = 0.82$, $p \ll 0.001$), affirming that BSi flux explains most of the variation in
1070 POC export fluxes at Z_{PAR} across the Atlantic and Indian sectors of the Great Calcite Belt
1071 region.

1072 The per-mole carrying capacities of BSi and PIC for POC, or the slopes m_{BSi} and
1073 m_{PIC} in the multiple linear regression Eq. (7), are 0.60 and 0.50, respectively. The per-
1074 weight carrying capacities of BSi and PIC for POC are 0.23 and 0.13, respectively,
1075 assuming $12 \times 2.199 \text{ g mol}^{-1}$ POC, $67.3 \text{ g SiO}_2 \cdot 0.4\text{H}_2\text{O mol}^{-1}$ BSi and 100.1 g CaCO_3
1076 mol^{-1} PIC (Klaas and Archer 2002). The unassociated POC flux, the constant in Eq. (7),
1077 is $1.7 \text{ mmol POC m}^{-2} \text{ d}^{-1}$, or $44 \text{ mg POC m}^{-2} \text{ d}^{-1}$. These carrying capacities for POC are 2-
1078 10 times higher than global biomineral carrying capacities of deeper ($>2000\text{m}$) flux data
1079 ($m_{\text{BSi}} = 0.025\text{-}0.026$, $m_{\text{PIC}} = 0.070\text{-}0.074$; Klaas and Archer, 2002), reflecting how POC
1080 remineralization with depth consistently reduces apparent mineral carrying capacities
1081 between the base of the euphotic zone and the deep sea.

1082 These upper ocean carrying capacities, especially m_{PIC} , are considerably different
1083 than corresponding per-weight carrying capacities reported in the *Crozex* study in the

Sarah Rosengard 5/18/15 6:15 PM
Deleted: , as defined by

Sarah Rosengard 5/18/15 6:16 PM
Deleted: , on a per-mole basis, and

Sarah Rosengard 5/18/15 6:18 PM
Deleted: , on a per-weight basis

Sarah Rosengard 5/18/15 6:22 PM
Deleted:

Sarah Rosengard 5/18/15 6:14 PM
Deleted: x 2.199

Sarah Rosengard 5/18/15 6:15 PM
Deleted: as defined by

1090 Indian sector of the Southern Ocean ($m_{BSi}= 0.16$, $m_{PIC}= -0.11$, constant=105 mg POC m⁻²
1091 d⁻¹) (Le Moigne et al., 2012). But, as the *Crozex* study was carried out several months
1092 earlier in the growing season than our sampling of the same area within the Great Calcite
1093 Belt, seasonal changes in the phytoplankton communities and their associated food webs
1094 could account for the differences in upper ocean carrying capacities. The Le Moigne et al.
1095 (2012) study also highlighted that variable ecosystem composition contributed to regional
1096 variations in upper ocean carrying capacities (Le Moigne et al. 2014), echoing a
1097 contemporaneous study that showed that even the deep (>1500 m) flux carrying
1098 capacities have statistically significant spatial variability (Wilson et al., 2012).

1099 It is worth noting that Le Moigne et al. (2012) included lithogenic minerals in
1100 their multiple linear regressions. We did not measure lithogenic minerals on GB1 and
1101 GB2, as we assumed lithogenic fluxes to be small in the Southern Ocean due to low
1102 terrestrial dust inputs (e.g., Honjo et al., 2000). While omitting this lithogenic component
1103 from the multiple linear regression could potentially impact derived m_{BSi} and m_{PIC} values,
1104 lithogenic material is nonetheless unlikely to be an important carrier of POC flux because
1105 of its low flux in the Southern Ocean. Indeed, regional studies have found that the
1106 lithogenic carrying capacity (Wilson et al., 2012) and the lithogenic-associated POC
1107 fluxes (Le Moigne et al., 2012) are very low in the Southern Ocean.

1108

1109 **4.6 Mineral-POC flux correlations in the mesopelagic zone**

1110

1111 To directly test whether minerals facilitate POC transfer through the upper
1112 mesopelagic zone of the water column as well, we compared flux transfer efficiencies
1113 100 m below the base of the euphotic zone (T_{100}) with BSi and PIC fluxes at z_{PAR} (Figs.
1114 9c, 9d). If the mineral ballast model were to apply to the upper mesopelagic zone, one
1115 would expect greater transfer efficiencies (i.e., lower attenuation of POC flux) in regions
1116 of higher mineral export. The data highlight several key differences between the role of
1117 minerals in the euphotic and upper mesopelagic zones. For one, the correlation between
1118 PIC flux and T_{100} , excluding values at GB1-25 and GB2-106, is significantly positive
1119 ($p<0.001$, $r^2=0.39$). The relationship remains even when assessing data from each cruise

1120 individually (for GB1, $p=0.047$, $r^2=0.34$; for GB2, $p=0.009$, $r^2=0.52$), lending further
1121 support to a potential role for PIC in POC transfer through the upper mesopelagic zone.

1122 Further, there was no significant correlation, with or without GB1-25 and GB2-
1123 106 T_{100} values, between BSi export fluxes in GB2 and T_{100} . However, higher particulate
1124 biogenic silica concentrations ($>51 \mu\text{m}$ [BSi]) at z_{PAR} did correspond with greater
1125 attenuation of $>51 \mu\text{m}$ [POC] below z_{PAR} ($p=0.004$, $r^2=0.35$; Fig. 10a), suggesting that in
1126 contrast to its role in the euphotic zone, BSi is associated with greater degradation in the
1127 mesopelagic zone of the water column.

1128

1129 4.7 Other controls on POC transfer

1130

1131 The correlation between the attenuation of $>51 \mu\text{m}$ [POC] and the size
1132 fractionation of POC ($\% >51 \mu\text{m}$ [POC]) at z_{PAR} is even stronger than with $>51 \mu\text{m}$ [BSi]
1133 ($p \ll 0.001$, $r^2=0.63$; Fig. 10b). GB1-85 appears to be an outlier for both relationships in
1134 Fig. 10, but especially for the relationship between $>51 \mu\text{m}$ [POC] attenuation and >51
1135 μm [BSi] (Fig. 10a). The correlation remains significant when the high [BSi] value from
1136 station GB1-85 is removed. Notably, the power law fit at GB1-85 is not very good in the
1137 upper mesopelagic; fitting $>51 \mu\text{m}$ [POC] between z_{PAR} and 500 m yields a better fit
1138 (higher r^2 ; see Fig. 3) with a higher attenuation coefficient of 2.35 (compared to 1.7 for
1139 the entire mesopelagic zone). This modified upper mesopelagic attenuation at GB1-85
1140 improves the overall correlations between the attenuation coefficient and both $>51 \mu\text{m}$
1141 [BSi] ($p \ll 0.001$, $r^2=0.60$) and $\% >51 \mu\text{m}$ [POC] ($p \ll 0.001$; $r^2=0.78$), further
1142 strengthening the argument that $>51 \mu\text{m}$ [BSi] and $\% >51 \mu\text{m}$ [POC] at z_{PAR} are
1143 important factors in POC transfer in the upper mesopelagic zone.

1144 The relationships between the attenuation of $>51 \mu\text{m}$ [POC] and $>51 \mu\text{m}$ [BSi]
1145 and particle size fractionation may arise from a more fundamental feature shared by both
1146 high-[BSi] and large-particle stations of the Great Calcite Belt: diatom-rich
1147 phytoplankton communities. Indeed, we also observe a strong correlation between >51
1148 μm [BSi] and $\% >51 \mu\text{m}$ [POC] at z_{PAR} ($p \ll 0.001$, $r^2=0.65$; not shown). This is a
1149 consistent feature across diatom-rich populations, which produce large, BSi-rich organic
1150 aggregates that sink rapidly out of the euphotic zone (Michaels and Silver, 1988;

Sarah Rosengard 5/21/15 3:42 PM

Deleted: -rich

Sarah Rosengard 5/20/15 5:50 PM

Deleted: dominated

1153 | Buesseler, 1998; Thomalla et al. 2006). Indeed, euphotic zone diatom abundances
1154 | enumerated with a FlowCam® are significantly correlated with >51 µm [BSi] at zPAR at
1155 | corresponding stations in GB1 and GB2 (see supplement; Fig. S2a). Thus, characteristics
1156 | describing ecosystem structure may underlie the correlation between BSi export and POC
1157 | export in the Great Calcite Belt (Francois et al. 2002; Thomalla et al., 2008; Henson et
1158 | al., 2012a; Henson et al., 2012b).

1159 | However, ecosystem composition does not directly explain why larger particles
1160 | exported into the mesopelagic zone are remineralized more vigorously hundreds of
1161 | meters below (Fig. 10b). It is paradoxical that the same large particles that sink quickly
1162 | out of the euphotic zone would then remineralize faster, as well. This association between
1163 | attenuation coefficient and particle size suggests that these particles sink more slowly
1164 | than expected in the mesopelagic zone given their size (for example, as a result of high
1165 | porosity and low excess density), and/or that they are subject to faster remineralization
1166 | compared to regions with more POC in the small size fraction. Francois et al. (2002)
1167 | noted a negative relationship between bathypelagic transfer efficiency and opal flux, and
1168 | attributed this to increased lability in large diatom aggregates. Though we do not observe
1169 | any negative correlation between upper mesopelagic transfer efficiency (T_{100}) and BSi
1170 | fluxes at z_{PAR} , we suggest that potentially higher degradability of POC produced by
1171 | diatom-rich communities may similarly explain the relationship between particle size and
1172 | >51 µm [POC] attenuation in the upper mesopelagic zone.

1173 | The view of POC quality as a driving factor behind POC transfer argues for a
1174 | deterministic role of euphotic zone community structure in POC transfer below the
1175 | euphotic zone. It supports the conventional perspective that diatom-dominated
1176 | communities are strong exporters of large, sinking POC particles out of the euphotic zone
1177 | (Buesseler, 1998; Guidi et al., 2009), but also adds to the growing view that these
1178 | communities have poor transfer efficiency and high attenuation through the mesopelagic
1179 | zone (Francois et al., 2002; Guidi et al., 2009; Henson et al., 2012b; Henson et al.,
1180 | 2012a).

1181 | For instance, station GB1-85, with over half of [POC] in the >51 µm size class
1182 | fraction in the euphotic zone (Fig. 6c; Table 3), has a low >51 µm [PIC]:[BSi] ratio of
1183 | 0.035 at z_{PAR} (indicated in log-scale in Figs. 10a and 10b), which indicates relatively high

Sarah Rosengard 5/20/15 5:50 PM

~~Deleted: dominated~~

Sarah Rosengard 5/20/15 5:44 PM

~~Deleted: a community dominated by~~

1186 | diatom **populations** producing large BSi-rich aggregates (Figs. 2, **S2, S3**). Station GB1-85
1187 | exhibits a high export efficiency (Ez-ratio= 0.38, within the upper quartile of the data
1188 | set), and the highest >51 μm [POC] and export fluxes at z_{PAR} (Figs. 5b, 7b, 8a; Table 3).
1189 | Notably, >51 μm [POC] values in the lower mesopelagic zone are also the highest at
1190 | GB1-85, despite attenuating greatly below z_{PAR} (attenuation coefficient = 1.7) (Figs. 3,
1191 | 8b, 8c; Table 2). But, because of high attenuation, proportionally less organic carbon
1192 | transfers to the deep sea at GB1-85. The same diatom-rich communities that vigorously
1193 | export POC **ultimately** may not sequester as much organic carbon in the deep ocean or
1194 | draw down as much atmospheric CO_2 (Kwon et al., 2009) as would be expected
1195 | considering the magnitude of export alone.

Sarah Rosengard 5/20/15 5:44 PM

Deleted: s

Sarah Rosengard 5/15/15 11:12 AM

Deleted: also have a short length scale of remineralization, and

1196 | In contrast to **a** model diatom community **like station GB1-85**, station GB1-25 is
1197 | BSi-deplete, with a >51 μm [PIC]:[BSi] ratio of **1.4** at z_{PAR} (indicated in log-scale in Fig.
1198 | 10a), indicating **relatively more** coccolithophores **in the community** (Figs. **S2, S3**). With
1199 | proportionally less POC in the >51 μm size-fraction (only 3.2%) (Figs. 6c, 10b; Table 3),
1200 | >51 μm [POC] at GB1-25 attenuates little through the mesopelagic zone (attenuation
1201 | coefficient = 0.4, the lowest of the data set) such that a third of the >51 μm [POC] at z_{PAR}
1202 | remains at 1000m, compared to only 1.4% at station GB1-85 (Fig. 3). At GB1-25, export
1203 | efficiency is very low (Ez-ratio=0.04), suggesting that the particles exiting the euphotic
1204 | zone here have been recycled vigorously in the euphotic zone prior to export, which may
1205 | explain their low >51 μm [POC] and high proportion in the <51 μm size-fraction at z_{PAR} .
1206 | In the mesopelagic zone, these particles are not very reactive and thus remineralize very
1207 | little, perhaps sequestering a higher proportion of the CO_2 fixed in the euphotic zone.

Sarah Rosengard 5/19/15 1:58 PM

Deleted: the

Sarah Rosengard 5/20/15 5:46 PM

Deleted: 4

Sarah Rosengard 5/20/15 5:48 PM

Deleted: the dominance

Sarah Rosengard 5/20/15 5:47 PM

Deleted: of

Sarah Rosengard 5/20/15 5:48 PM

Deleted: over

Sarah Rosengard 5/20/15 5:48 PM

Deleted: diatoms

1208 | Several other stations with proportionally more small particles and weaker >51
1209 | μm [POC] attenuation in the mesopelagic zone exhibit higher >51 μm [PIC] than >51 μm
1210 | [BSi] at z_{PAR} (labeled in the lower left quadrant of Fig. 10b), suggesting that export
1211 | regimes **characterized** by **high relative abundance of** coccolithophores **consistently**
1212 | transfer less reactive POC to the mesopelagic zone. Artificial roller tank experiments
1213 | have demonstrated that coccolithophore cultures can produce smaller, more compact
1214 | aggregates than diatom cultures, partly because of smaller cell sizes (Iversen and Ploug,
1215 | 2010). However, smaller size does not necessarily mean slower sinking velocities (e.g.,
1216 | McDonnell and Buesseler, 2010). Iversen and Ploug (2010) showed that the higher

Sarah Rosengard 5/20/15 5:50 PM

Deleted: dominated

Sarah Rosengard 5/20/15 5:50 PM

Deleted: over diatoms

1228 excess density of these small aggregates generated faster sinking speeds than similarly
1229 sized pure diatom aggregates. Another roller tank study that compared aggregate
1230 formation by calcifying versus non-calcifying coccolithophores observed that aggregates
1231 formed from calcifying coccolithophores were smaller but faster sinking (Engel et al.,
1232 2009). In regions like the Great Calcite Belt, dense coccolithophore populations may
1233 similarly export small, highly degraded and compact particles out of the euphotic zone.
1234 As a result, these communities would efficiently transfer POC towards the base of the
1235 mesopelagic zone, even if the magnitude of exported POC is not as high as in diatom-rich
1236 regions (Thomalla et al., 2008; Guidi et al., 2009; Henson et al., 2012b). This may
1237 explain why higher PIC export fluxes are associated with higher transfer efficiencies but
1238 not higher POC flux at z_{PAR} (Fig. 9), and also why the ballast association between PIC
1239 and POC fluxes appears only at greater depths (Francois et al., 2002; Klaas and Archer,
1240 2002).

1241 Attenuation coefficients for $>51 \mu\text{m}$ [POC] across diatom-rich regions exhibit a
1242 great spread (standard deviation= 0.47), ranging from 0.47 to 1.88. Not all diatom-rich
1243 stations (i.e., $>51 \mu\text{m}$ [PIC]:[BSi] <1 at z_{PAR}) have proportionally larger particles or higher
1244 b-values (e.g., stations GB1-70, GB1-77 and GB2-87; Fig. 10b). In contrast, attenuation
1245 coefficients across coccolithophore-rich regions (i.e., $>51 \mu\text{m}$ [PIC]:[BSi] ≥ 1 at z_{PAR})
1246 exhibit a lower standard deviation (0.31) and a smaller range, 0.35 to 1.12. The greater
1247 variance in attenuation across BSi-rich regions may result from sampling the diatom
1248 populations at different seasons of the bloom cycle (Lam et al., 2011), and implies that
1249 there may be less seasonality in POC transfer to depth in coccolithophore-rich regions.
1250 Indeed, massive diatom export events with high transfer efficiency through the
1251 mesopelagic zone have been observed (Martin et al., 2011; Smetacek et al. 2012), so
1252 there are clearly conditions that can lead to efficient mesopelagic POC transfer from
1253 diatom blooms.

1254 It is worth noting that $>51 \mu\text{m}$ [PIC]:[BSi] ratios did increase with depth at most
1255 stations of the Great Calcite Belt, as might be expected because BSi is undersaturated in
1256 seawater. The possibility that BSi dissolves faster than PIC in particles sinking through
1257 the mesopelagic zone would complicate the connections we draw between diatom-rich
1258 communities in the euphotic zone and the attenuation of $>51 \mu\text{m}$ [POC]. But, there are no

Sarah Rosengard 5/15/15 11:12 AM
Deleted: the remineralization length scale of calcareous assemblages is likely to be longer than regions dominated by diatom assemblages. T

Sarah Rosengard 5/20/15 5:50 PM
Deleted: dominated

Sarah Rosengard 5/20/15 5:51 PM
Deleted: dominated

Sarah Rosengard 5/20/15 5:52 PM
Deleted: ,

Sarah Rosengard 5/20/15 5:52 PM
Deleted: such that n

Sarah Rosengard 5/20/15 5:52 PM
Deleted: dominated by diatoms

Sarah Rosengard 5/20/15 5:51 PM
Deleted: dominated

Sarah Rosengard 5/20/15 5:53 PM
Deleted: dominated

Sarah Rosengard 5/20/15 5:53 PM
Deleted: dominated

1271 associations between the magnitude of [PIC]:[BSi] increase and $>51 \mu\text{m}$ [BSi] at Z_{PAR} ,
1272 $>51 \mu\text{m}$ [PIC] at Z_{PAR} or $>51 \mu\text{m}$ [POC] attenuation with depth, suggesting that the issue
1273 of differential dissolution should not significantly impact our earlier interpretations. In
1274 the future, directly evaluating the degradability of sinking POC using organic
1275 characterization techniques (e.g., ramped pyrolysis or biomarker isolation) (e.g.,
1276 Wakeham et al., 2002; Rosenheim et al., 2008; Rosenheim and Galy, 2012; Rosenheim et
1277 al., 2013) would greatly improve our ability to track the transformation of POC produced
1278 by different ecosystem assemblages across the Great Calcite Belt.

1279

1280 **5 Conclusion**

1281

1282 In summary, we argue here that phytoplankton assemblages play a fundamental
1283 role (Francois et al., 2002; Thomalla et al., 2008; Henson et al., 2012b; Henson et al.,
1284 2012a) in determining the fate of POC export through the Great Calcite Belt region, the
1285 effect of which sometimes, but not always, appears as a mineral ballast mechanism in the
1286 euphotic zone (Lam et al., 2011; Henson et al., 2012a; Lima et al., 2013). Though
1287 shallow BSi export fluxes were strongly correlated with POC export fluxes, they are also
1288 associated with diatom communities that produce larger particles that attenuate more
1289 quickly through the mesopelagic zone, such that proportionally less POC reaches the
1290 lower mesopelagic zone, and proportionally more is returned to the water column as
1291 remineralized carbon (dissolved inorganic and organic carbon).

1292

1293 **Author contributions:**

1294 S.Z. Rosengard, the primary author, participated in the GB2 field work, sample analysis
1295 in lab and writing. P.J. Lam contributed to field work during GB2, and participated in
1296 both data interpretation and editing the manuscript. W.M. Balch, supplied the primary
1297 productivity and light profile data included here, and provided valuable feedback during
1298 writing. M.E. Auro and S. Pike participated in field work and sample analysis during and
1299 after GB1. D. Drapeau and B. Bowler contributed to field work during both GB1 and
1300 GB2, as well as sample analysis, particularly with respect to primary productivity and
1301 light profile data.

1302

1303 **Acknowledgements:**

1304 Many thanks to Ken Buesseler for discussions and lending us field equipment; Dan
1305 Ohnemus, Angela Warner, Michael Brown, Rebecca Fowler, and Marina Van der Eb for
1306 help at sea; and Laura Lubelczyk, Paul Henderson, and Scott Birdwhistell for analytical
1307 work/assistance. This work was funded by NSF OCE-0960880 to P.J. Lam, and NSF
1308 OCE-0961660, NASA NNX11A072G and NNX11AL93G to W.M. Balch.

1309

1310 **References**

1311

1312 Abramson, L., Lee, C., Liu, Z. F., Wakeham, S. G., and Szlosek, J.: Exchange between
1313 suspended and sinking particles in the northwest Mediterranean as inferred from
1314 the organic composition of in situ pump and sediment trap samples, *Limnology*
1315 and *Oceanography*, 55, 725-739, 2010.

1316

1317 Armstrong, R. A., Lee, C., Hedges, J. I., Honjo, S., and Wakeham, S. G.: A new,
1318 mechanistic model for organic carbon fluxes in the ocean based on the
1319 quantitative association of POC with ballast minerals, *Deep-Sea Research Part II-*
1320 *Topical Studies in Oceanography*, 49, 219-236, 2002.

1321

1322 Balch, W. M., Drapeau, D., and Fritz, J.: Monsoonal forcing of calcification in the
1323 Arabian Sea, *Deep-Sea Research II*, 47, 1301-1337, 2000.

1324

1325 Balch, W. M., Drapeau, D. T., Bowler, B. C., Lyczkowski, E. R., Lubelczyk, L. C.,
1326 Painter, S. C., and Poulton, A. J.: Surface biological, chemical, and optical
1327 properties of the Patagonian Shelf coccolithophore bloom, the brightest waters of
1328 the Great Calcite Belt, *Limnology and Oceanography*, 59, 1715-1732, 2014.

1329

1330 Balch, W. M., Drapeau, D. T., Bowler, B. C., Lyczkowski, E., Booth, E. S., and Alley,
1331 D.: The contribution of coccolithophores to the optical and inorganic carbon
1332 budgets during the Southern Ocean Gas Exchange Experiment: New evidence in
1333 support of the Great Calcite Belt hypothesis, *J. Geophys. Res.*, 116, C00F06,
1334 2011a.

1335

1336 Balch, W. M., Poulton, A. J., Drapeau, D. T., Bowler, B. C., Windecker, L. A., and
1337 Booth, E. S.: Zonal and meridional patterns of phytoplankton biomass and carbon
1338 fixation in the Equatorial Pacific Ocean, between 110°W and 140°W, *Limnology*
1339 and *Oceanography*, 59, 1715-1732, 2011b.

1340

1341 Belkin, I. M. and Gordon, A. L.: Southern Ocean fronts from the Greenwich meridian to
 1342 Tasmania, *Journal of Geophysical Research: Oceans* (1978–2012), 101, 3675-
 1343 3696, 1996.
 1344

1345 Bishop, J. K. B., Lam, P. J., and Wood, T. J.: Getting good particles: accurate sampling
 1346 of particles by large volume in-situ filtration, *Limnology and Oceanography*
 1347 *Methods*, 10, 681-710, 2012.
 1348

1349 Brzezinski, M. A. and Nelson, D. M.: Seasonal changes in the silicon cycle within a Gulf
 1350 Stream warm-core ring, *Deep Sea Research Part A. Oceanographic Research*
 1351 *Papers*, 36, 1009-1030, 1989.
 1352

1353 Buesseler, K., Lamborg, C. H., Cai, P., Escoube, R., Johnson, R., Pike, S., Masque, P.,
 1354 McGillicuddy, D., and Verdeny, E.: Particle fluxes associated with mesoscale
 1355 eddies in the Sargasso Sea, *Deep-Sea Research II*, 55, 1426-1444, 2008.
 1356

1357 Buesseler, K. O.: The decoupling of production and particulate export in the surface
 1358 ocean, *Global Biogeochemical Cycles*, 12, 297-310, 1998.
 1359

1360 Buesseler, K. O., Ball, L., Andrews, J., Cochran, J. K., Hirschberg, D. J., Bacon, M. P.,
 1361 Fler, A., and Brzezinski, M.: Upper ocean export of particulate organic carbon
 1362 and biogenic silica in the Southern Ocean along 170 degrees W, *Deep-Sea*
 1363 *Research Part II-Topical Studies in Oceanography*, 48, 4275-4297, 2001.
 1364

1365 Buesseler, K. O., Barber, R. T., Dickson, M. L., Hiscock, M. R., Moore, J. K., and
 1366 Sambrotto, R.: The effect of marginal ice-edge dynamics on production and
 1367 export in the Southern Ocean along 170 degrees W, *Deep-Sea Research Part II-*
 1368 *Topical Studies in Oceanography*, 50, 579-603, 2003.
 1369

1370 Buesseler, K. O., Benitez-Nelson, C. R., Moran, S. B., Burd, A., Charette, M., Cochran,

Sarah Rosengard 5/21/15 9:43 AM
 Deleted: i

1372 J. K., Coppola, L., Fisher, N. S., Fowler, S. W., and Gardner, W. D.: An
1373 assessment of particulate organic carbon to thorium-234 ratios in the ocean and
1374 their impact on the application of ^{234}Th as a POC flux proxy, *Marine Chemistry*,
1375 100, 2006.
1376
1377 Buesseler, K. O. and Boyd, P.: Shedding light on processes that control particle export
1378 and flux attenuation in the twilight zone of the open ocean, *Limnol, Oceanogr*, 54,
1379 1210-1232, 2009.
1380
1381 Buesseler, K. O., Lamborg, C. H., Boyd, P. W., Lam, P. J., Trull, T. W., Bidigare, R. R.,
1382 Bishop, J. K. B., Casciotti, K. L., Dehairs, F., Elskens, M., Honda, M., Karl, D.
1383 M., Siegel, D. A., Silver, M. W., Steinberg, D. K., Valdes, J., Van Mooy, B., and
1384 Wilson, S.: Revisiting carbon flux through the ocean's twilight zone, *Science*,
1385 316, 567-570, 2007.
1386
1387 Buesseler, K. O., Pike, S., Maiti, K., Lamborg, C. H., Siegel, D. A., and Trull, T. W.:
1388 Thorium-234 as a tracer of spatial, temporal and vertical variability in particle
1389 flux in the North Pacific, *Deep Sea Research Part I: Oceanographic Research*
1390 *Papers*, 56, 1143-1167, 2009.
1391
1392 Cochran, J. K., Buesseler, K. O., Bacon, M. P., Wang, H. W., Hirschberg, D. J., Ball, L.,
1393 Andrews, J., Crossin, G., and Fleer, A.: Short-lived thorium isotopes (Th-234, Th-
1394 228) as indicators of POC export and particle cycling in the Ross Sea, Southern
1395 Ocean, *Deep-Sea Research Part Ii-Topical Studies in Oceanography*, 47, 3451-
1396 3490, 2000.
1397
1398 Coppola, L., Roy-Barman, M., Mulsow, S., Povinec, P., and Jeandel, C.: Low particulate
1399 organic carbon export in the frontal zone of the Southern Ocean (Indian sector)
1400 revealed by Th-234, *Deep-Sea Research Part I-Oceanographic Research Papers*,
1401 52, 51-68, 2005.
1402

1403 De La Rocha, C. L., Nowald, N., and Passow, U.: Interactions between diatom
1404 aggregates, minerals, particulate organic carbon, and dissolved organic matter:
1405 Further implications for the ballast hypothesis, *Global Biogeochemical Cycles*,
1406 22, 2008.
1407
1408 Engel, A., Szlosek, J., Abramson, L., Liu, Z., and Lee, C.: Investigating the effect of
1409 ballasting by CaCO₃ in *Emiliana huxleyi*: I. Formation, settling velocities and
1410 physical properties of aggregates, *Deep Sea Research Part II: Topical Studies in*
1411 *Oceanography*, 56, 1396-1407, 2009.
1412
1413 Fabry, V. J. and Balch, W. M.: Direct measurements of calcification rates in planktonic
1414 organisms., U. Riebesell, V.J. Fabry, L. Hansson and J.-P. Gattuso (Editors),
1415 Guide to Best Practices in Ocean Acidification Research and Data Reporting.
1416 European Project on Ocean Acidification (EPOCA), Bremerhaven, Germany,
1417 2010. 185-196, 2010.
1418
1419 Francois, R., Honjo, S., Krishfield, R., and Manganini, S.: Factors controlling the flux of
1420 organic carbon to the bathypelagic zone of the ocean, *Global Biogeochemical*
1421 *Cycles*, 16, 1087, doi:10.1029/2001GB001722, 2002.
1422
1423 Friedrich, J. and van der Loeff, M. M. R.: A two-tracer (Po-210-Th-234) approach to
1424 distinguish organic carbon and biogenic silica export flux in the Antarctic
1425 Circumpolar Current, *Deep-Sea Research Part I-Oceanographic Research Papers*,
1426 49, 101-120, 2002.
1427
1428 Giering, S. L. C., Sanders, R., Lampitt, R. S., Anderson, T. R., Tamburini, C., Boutrif,
1429 M., Zubkov, M. V., Marsay, C. M., Henson, S. A., Saw, K., Cook, K., and Mayor,
1430 D. J.: Reconciliation of the carbon budget in the ocean's twilight zone, *Nature*,
1431 507, 480-483, 2014.
1432
1433 Glover, D. M., Jenkins, W. J., and Doney, S. C.: Modeling methods for marine science.,

1434 | Cambridge University Press, New York, 2011. ▾
1435
1436 Guidi, L., Stemmann, L., Jackson, G. A., Ibanez, F., Claustre, H., Legendre, L., Picheral,
1437 M., and Gorsky, G.: Effects of phytoplankton community on production, size and
1438 export of large aggregates: A world-ocean analysis, *Limnology and*
1439 *Oceanography*, 54, 1951-1963, 2009.
1440
1441 Hedges, J. I. and Oades, J. M.: Comparative organic geochemistries of soils and marine
1442 sediments, *Organic Geochemistry*, 27, 319-361, 1997.
1443
1444 Henson, S., Lampitt, R., and Johns, D.: Variability in phytoplankton community structure
1445 in response to the North Atlantic Oscillation and implications for organic carbon
1446 flux, *Limnology and Oceanography*, 57, 1591, 2012a.
1447
1448 Henson, S. A., Sanders, R., and Madsen, E.: Global patterns in efficiency of particulate
1449 organic carbon export and transfer to the deep ocean, *Global Biogeochem. Cycles*,
1450 26, GB1028, 2012b.
1451
1452 Henson, S. A., Sanders, R., Madsen, E., Morris, P. J., Le Moigne, F., and Quartly, G. D.:
1453 A reduced estimate of the strength of the ocean's biological carbon pump,
1454 *Geophys. Res. Lett.*, 38, L04606, 2011.
1455 |
1456 [Henson, S. A., Yool, A., and Sanders, R.: Variability in efficiency of particulate organic](#)
1457 [carbon export: A model study, *Global Biogeochem. Cycles*, 29, GB004965, 2015.](#) ▸
1458
1459 Honjo, S., Francois, R., Manganini, S., Dymond, J., and Collier, R.: Particle fluxes to the
1460 interior of the Southern Ocean in the Western Pacific sector along 170 degrees W,
1461 *Deep-Sea Research Part Ii-Topical Studies in Oceanography*, 47, 3521-3548,
1462 2000.
1463
1464 Iversen, M. H. and Ploug, H.: Ballast minerals and the sinking carbon flux in the ocean:

Sarah Rosengard 5/21/15 12:31 PM
Deleted: 2011.

Sarah Rosengard 5/21/15 9:46 AM
Formatted: Indent: First line: 0.5"

1466 carbon-specific respiration rates and sinking velocity of marine snow aggregates,
1467 Biogeosciences, 7, 2613-2624, 2010.
1468
1469 Jacquet, S. H. M., Lam, P. J., Trull, T., and Dehairs, F.: Carbon export production in the
1470 subantarctic zone and polar front zone south of Tasmania, Deep Sea Research
1471 Part II: Topical Studies in Oceanography, 58, 2277-2292, 2011.
1472
1473 Klaas, C. and Archer, D. E.: Association of sinking organic matter with various types of
1474 mineral ballast in the deep sea: Implications for the rain ratio, Global
1475 Biogeochemical Cycles, 16, 1116-1129, 2002.
1476
1477 Kwon, E. Y., Primeau, F., and Sarmiento, J. L.: The impact of remineralization depth on
1478 the air-sea carbon balance, Nature Geoscience, 2, 630-635, 2009.
1479
1480 Lam, P. J. and Bishop, J. K. B.: High biomass, low export regimes in the Southern
1481 Ocean, Deep Sea Research Part II: Topical Studies in Oceanography, 54, 601-
1482 638, 2007.
1483
1484 Lam, P. J., Doney, S. C., and Bishop, J. K. B.: The dynamic ocean biological pump:
1485 Insights from a global compilation of particulate organic carbon, CaCO₃, and opal
1486 concentration profiles from the mesopelagic, Global Biogeochem. Cycles, 25,
1487 GB3009, 2011.
1488
1489 Lam, P. J., Ohnemus, D. C., and Auro, M. E.: Size-fractionated major particle
1490 composition and concentrations from the US GEOTRACES north Atlantic zonal
1491 transect, Deep Sea Research Part II: Topical Studies in Oceanography, 2014.
1492 2014.
1493
1494 Le Moigne, F., Henson, S., Sanders, R., and Madsen, E.: Global database of surface
1495 ocean particulate organic carbon export fluxes diagnosed from the 234 Th
1496 technique, Earth System Science Data Discussions, 6, 163-187, 2013.

1497
1498 Le Moigne, F. A. C., Pabortsava, K., Marcinko, C. L. J., Martin, P., and Sanders, R. J.:
1499 Where is mineral ballast important for surface export of particulate organic
1500 carbon in the ocean?, *Geophysical Research Letters*, doi:
1501 10.1002/2014GL061678, 2014. 2014GL061678, 2014.
1502
1503 Le Moigne, F. A. C., Sanders, R. J., Villa-Alfageme, M., Martin, A. P., Pabortsava, K.,
1504 Planquette, H., Morris, P. J., and Thomalla, S. J.: On the proportion of ballast
1505 versus non-ballast associated carbon export in the surface ocean, *Geophys. Res.*
1506 *Let.*, 39, L15610, 2012.
1507
1508 Lima, I. D., Lam, P. J., and Doney, S. C.: Dynamics of particulate organic carbon flux in
1509 a global ocean model, *Biogeosciences Discuss.*, 10, 14715-14767, 2013.
1510
1511 Lomas, M. W., Steinberg, D. K., Dickey, T., Carlson, C. A., Nelson, N. B., Condon, R.
1512 H., and Bates, N. R.: Increased ocean carbon export in the Sargasso Sea linked to
1513 climate variability is countered by its enhanced mesopelagic attenuation,
1514 *Biogeosciences*, 7, 57-70, 2010.
1515
1516 Maiti, K., Benitez-Nelson, C. R., [Rii, Y., and Bidigare, R.: The influence of a mature](#)
1517 [cyclonic eddy on particle export in the lee of Hawaii](#), *Deep Sea Research Part II:*
1518 *Topical Studies in Oceanography*, 55, 1445-1560, 2012.
1519
1520 Martin, J. H., Knauer, G. A., Karl, D. M., and Broenkow, W. W.: Vertex - Carbon
1521 Cycling in the Northeast Pacific, *Deep-Sea Research Part a-Oceanographic*
1522 *Research Papers*, 34, 267-285, 1987.
1523
1524 Martin, P., Lampitt, R. S., Jane Perry, M., Sanders, R., Lee, C., and D'Asaro, E.: Export
1525 and mesopelagic particle flux during a North Atlantic spring diatom bloom, *Deep*
1526 *Sea Research Part I: Oceanographic Research Papers*, 58, 338-349, 2011.
1527

Sarah Rosengard 5/18/15 3:33 PM
Deleted: and Buesseler, K. O.

Sarah Rosengard 5/18/15 3:34 PM
Deleted: Insights into particle formati ... [1]

Sarah Rosengard 5/18/15 3:34 PM
Deleted: , Thoruim-234

Sarah Rosengard 5/18/15 3:34 PM
Deleted: Geophysical Research Letters

Sarah Rosengard 5/18/15 3:34 PM
Deleted: 37

Sarah Rosengard 5/18/15 3:33 PM
Deleted: 2010

1535 McCave, I. N.: Vertical flux of particles in the ocean, *Deep Sea Research*, 22, 491-502,
1536 1975.
1537

1538 McDonnell, A. M. P. and Buesseler, K. O.: Variability in the average sinking velocities
1539 of marine particles, *Limnology and Oceanography*, 55, 2085-2096, 2010.
1540

1541 Michaels, A. F. and Silver, M. W.: Primary production, sinking fluxes and the microbial
1542 food web, *Deep Sea Research Part A. Oceanographic Research Papers*, 35, 473-
1543 490, 1988.
1544

1545 Morris, P. J., Sanders, R., Turnewitsch, R., and Thomalla, S.: Th-234-derived particulate
1546 organic carbon export from an island-induced phytoplankton bloom in the
1547 Southern Ocean, *Deep-Sea Research Part Ii-Topical Studies in Oceanography*, 54,
1548 2208-2232, 2007.
1549

1550 Owens, S., Buesseler, K., and Sims, K.: Re-evaluating the ^{238}U -salinity relationship in
1551 seawater: Implications for the ^{238}U - ^{234}Th disequilibrium method, *Marine*
1552 *Chemistry*, 127, 31-39, 2011.
1553

1554 Paasche, E. and Brubak, S.: Enhanced calcification in the coccolithophorid *Emiliana*
1555 *huxleyi* (Haptophyceae) under phosphorus limitation, *Phycologia*, 33, 324-330,
1556 1994.
1557

1558 Passow, U. and De la Rocha, C. L.: Accumulation of mineral ballast on organic
1559 aggregates, *Global Biogeochemical Cycles*, 20, 2006.
1560

1561 Pike, S. M., Buesseler, K. O., Andrews, J., and Savoye, N.: Quantification of Th-234
1562 recovery in small volume sea water samples by inductively coupled plasma-mass
1563 spectrometry, *Journal of Radioanalytical and Nuclear Chemistry*, 263, 355-360,
1564 2005.
1565

1566 Pilson, M. E. Q.: An Introduction to the Chemistry of the Sea, Cambridge University
1567 Press, New York, 2012. 2012.
1568

1569 Planchon, F., Cavagna, A.-J., Cardinal, D., André, L., and Dehairs, F.: Late summer
1570 particulate organic carbon export and twilight zone remineralisation in the
1571 Atlantic sector of the Southern Ocean, *Biogeosciences*, 10, 803-820, 2013.
1572

1573 Resplandy, L., Martin, A. P., Le Moigne, F., Martin, P., Aquilina, A., Mémery, L., Lévy,
1574 M., and Sanders, R.: How does dynamical spatial variability impact ^{234}Th -derived
1575 estimates of organic export?, *Deep Sea Research Part I: Oceanographic Research*
1576 *Papers*, 68, 24-45, 2012.
1577

1578 Riley, J. S., Sanders, R., Marsay, C., Le Moigne, F. A. C., Achterberg, E. P., and Poulton,
1579 A. J.: The relative contribution of fast and slow sinking particles to ocean carbon
1580 export, *Global Biogeochem. Cycles*, 26, GB1026, 2012.
1581

1582 Rodriguez y Baena, A. M., Boudjenoun, R., Fowler, S. W., Miquel, J. C., Masqué, P.,
1583 Sanchez-Cabeza, J.-A., and Warnau, M.: ^{234}Th -based carbon export during an ice-
1584 edge bloom: Sea-ice algae as a likely bias in data interpretation, *Earth and*
1585 *Planetary Science Letters*, 269, 596-604, 2008.
1586

1587 Rosenheim, B. E., Day, M. B., Domack, E., Schrum, H., Benthien, A., and Hayes, J. M.:
1588 Antarctic sediment chronology by programmed-temperature pyrolysis:
1589 Methodology and data treatment, *Geochemistry, Geophysics, Geosystems*, 9,
1590 2008.
1591

1592 Rosenheim, B. E. and Galy, V.: Direct measurement of riverine particulate organic
1593 carbon age structure, *Geophysical Research Letters*, 39, 2012.
1594

1595 Rosenheim, B. E., Roe, K. M., Roberts, B. J., Kolker, A. S., Allison, M. A., and

1596 Johannesson, K. H.: River discharge influences on particulate organic carbon age
1597 structure in the Mississippi/Atchafalaya River System, *Global Biogeochemical*
1598 *Cycles*, 27, 154-166, 2013.

1599

1600 Rutgers van der Loeff, M. M., Cai, P. H., Stimac, I., Bracher, A., Middag, R., Klunder,
1601 M. B., and van Heuven, S. M.: ^{234}Th in surface waters: Distribution of particle
1602 export flux across the Antarctic Circumpolar Current and in the Weddell Sea
1603 during the GEOTRACES expedition ZERO and DRAKE, *Deep Sea Research*
1604 *Part II: Topical Studies in Oceanography*, 58, 2749-2766, 2011.

1605

1606 Rutgers Van Der Loeff, M. M., Friedrich, J., and Bathmann, U. V.: Carbon export during
1607 the Spring Bloom at the Antarctic Polar Front, determined with the natural tracer
1608 ^{234}Th , *Deep Sea Research Part II: Topical Studies in Oceanography*, 44, 457-478,
1609 1997.

1610

1611 Rutgers van der Loeff, M. M., Sarin, M. M., Baskaran, M., Benitez-Nelson, C.,
1612 Buesseler, K. O., Charette, M., Dai, M., Gustafsson, r., Masque, P., Morris, P. J.,
1613 Orlandini, K., Rodriguez y Baena, A., Savoye, N., Schmidt, S., Turnewitsch, R.,
1614 V`ge, I., and Waples, J. T.: A review of present techniques and methodological
1615 advances in analyzing ^{234}Th in aquatic systems, *Marine Chemistry*, 100, 190-212,
1616 2006.

1617

1618 Sanders, R., Morris, P. J., Poulton, A. J., Stinchcombe, M. C., Charalampopoulou, A.,
1619 Lucas, M. I., and Thomalla, S. J.: Does a ballast effect occur in the surface
1620 ocean?, *Geophysical Research Letters*, 37, L08602, 2010.

1621

1622 Santschi, P., Murray, J. W., Baskaran, M., Benitez-Nelson, C. R., Guo, L., Hung, C.-C.,
1623 Lamborg, C., Moran, S. B., Passow, U., and Roy-Barman, M.: Thorium
1624 speciation in seawater, *Marine Chemistry*, 100, 250-268, 2006.

1625

1626 Sarmiento, J. L., Dunne, J., Gnanadesikan, A., Key, R. M., Matsumoto, K., and Slater,

1627 R.: A new estimate of the CaCO₃ to organic carbon export ratio, Global
1628 Biogeochemical Cycles, 16, 2002.

1629

1630 Sarmiento, J. L., Gruber, N., Brzezinski, M. A., and Dunne, J. P.: High-latitude controls
1631 of thermocline nutrients and low latitude biological productivity, Nature, 427, 56-
1632 60, 2004.

1633

1634 Savoye, N., Benitez-Nelson, C., Burd, A. B., Cochran, J. K., Charette, M., Buesseler, K.
1635 O., Jackson, G. A., Roy-Barman, M., Schmidt, S., and Elskens, M.: Th-234
1636 sorption and export models in the water column: A review, Marine Chemistry,
1637 100, 234-249, 2006.

1638

1639 Savoye, N., Trull, T. W., Jacquet, S. H. M., Navez, J., and Dehairs, F.: ²³⁴Th-based
1640 export fluxes during a natural iron fertilization experiment in the Southern Ocean
1641 (KEOPS), Deep Sea Research Part II: Topical Studies in Oceanography, 55, 841-
1642 855, 2008.

1643

1644 Shimmiel, G. B., Ritchie, G. D., and Fileman, T. W.: The Impact of Marginal Ice-Zone
1645 Processes on the Distribution of Pb-210, Po-210 and Th-234 and Implications for
1646 New Production in the Bellingshausen Sea, Antarctica, Deep-Sea Research Part
1647 II-Topical Studies in Oceanography, 42, 1313-1335, 1995.

1648

1649 Smetacek, V., Klaas, C., Strass, V. H., Assmy, P., Montresor, M., Cisewski, B., Savoye,
1650 N., Webb, A., d'Odivio, F., Arrieta, J. M., Bathmann, U., Bellerby, R., Berg, G.
1651 M., Croot, P., Gonzalez, S., Henjes, J., Herndl, G. J., Hoffmann, L. J., Leach, H.,
1652 Losch, M., Mills, M. M., Neill, C., Peeken, I., Röttgers, R., Sachs, O., Sauter, E.,
1653 Schmidt, M. M., Schwarz, J., Terbrüggen, A., and Wolf-Gladrow, D.: Deep
1654 carbon export from a Southern Ocean iron-fertilized diatom bloom, Nature, 487,
1655 7407, 313-319, 2012.

1656

1657 Sokolov, S. and Rintoul, S. R.: Circumpolar structure and distribution of the Antarctic

1658 Circumpolar Current fronts: 1. Mean circumpolar paths, *Journal of Geophysical*
1659 *Research: Oceans* (1978–2012), 114, 2009.

1660 Steinberg, D. K., Van Mooy, B. A. S., Buesseler, K. O., Boyd, P. W., Kobari, T., and
1661 Karl, D. M.: Bacterial vs. zooplankton control of sinking particle flux in the
1662 ocean's twilight zone, *Limnology and Oceanography*, 53, 1327-1338, 2008.

1663

1664 Strickland, J. D. and Parsons, T. R.: A practical handbook of seawater analysis, Fisheries
1665 Research Board of Canada Ottawa, 1968.

1666

1667 Thomalla, S., Turnewitsch, R., Lucas, M., and Poulton, A.: Particulate organic carbon
1668 export from the North and South Atlantic gyres: The $^{234}\text{Th}/^{238}\text{U}$ disequilibrium
1669 approach, *Deep Sea Research Part II: Topical Studies in Oceanography*, 53, 1629-
1670 1648, 2006.

1671

1672 Thomalla, S. J., Poulton, A. J., Sanders, R., Turnewitsch, R., Holligan, P. M., and Lucas,
1673 M. I.: Variable export fluxes and efficiencies for calcite, opal, and organic carbon
1674 in the Atlantic Ocean: A ballast effect in action?, *Global Biogeochem. Cycles*, 22,
1675 GB1010, 2008.

1676

1677 Trull, T. W., Bray, S. G., Buesseler, K. O., Lamborg, C. H., Manganini, S., Moy, C., and
1678 Valdes, J.: In situ measurement of mesopelagic particle sinking rates and the
1679 control of carbon transfer to the ocean interior during the Vertical Flux in the
1680 Global Ocean (VERTIGO) voyages in the North Pacific, *Deep-Sea Research Part*
1681 *II-Topical Studies in Oceanography*, 55, 1684-1695, 2008.

1682

1683 Volk, T. and Hoffert, M. I.: Ocean carbon pumps: Analysis of relative strengths and
1684 efficiencies in ocean-driven atmospheric CO_2 changes, *Geophysical Monographs*,
1685 32, 99-110, 1985.

1686

1687 Wakeham, S. G., Peterson, M. L., Hedges, J. I., and Lee, C.: Lipid biomarker fluxes in

1688 the Arabian Sea, with a comparison to the equatorial Pacific Ocean, Deep-Sea
1689 Research Part II-Topical Studies in Oceanography, 49, 2265-2301, 2002.
1690
1691 Wilson, J. D., Barker, S., and Ridgwell, A.: Assessment of the spatial variability in
1692 particulate organic matter and mineral sinking fluxes in the ocean interior:
1693 Implications for the ballast hypothesis, Global Biogeochemical Cycles, 26,
1694 GB4011, 2012.
1695
1696 Wilson, S. E., Steinberg, D. K., and Buesseler, K. O.: Changes in fecal pellet
1697 characteristics with depth as indicators of zooplankton repackaging of particles in
1698 the mesopelagic zone of the subtropical and subarctic North Pacific Ocean, Deep-
1699 Sea Research Part II-Topical Studies in Oceanography, 55, 1636-1647, 2008.
1700
1701 Zhou, K., Nodder, S., Dai, M., and Hall, J.: Insignificant enhancement of export flux in
1702 the highly productive subtropical front, east of New Zealand: a high resolution
1703 study of particle export fluxes based on ^{234}Th : ^{238}U disequilibria, Biogeosciences,
1704 9, 973-992, 2012.
1705

1706 Table 1. Locations and times of sampling of total ^{234}Th and size-fractionated particles on
 1707 cruises GB1 and GB2. Two export depths are indicated: z_{PAR} (depth of 0.3% of surface
 1708 | photosynthetically available radiation) and $z_{\text{Th/U}}$ (depth where ^{234}Th and ^{238}U activities
 1709 return to secular equilibrium below surface deficits).

Sarah Rosengard 5/20/15 3:01 PM
 Deleted: active

1710

Cruise	Station	Date	Lat.	Long.	z_{PAR}	$z_{\text{Th/U}}$
-	-	dd-mm-yy	deg. N	deg. E	m	m
GB1	6	14 Jan 2011	-51.79	-56.11	79	130
GB1	16	17 Jan 2011	-46.26	-59.83	62	141
GB1	25	20 Jan 2011	-45.67	-48.95	62	115
GB1	32	22 Jan 2011	-40.95	-46.00	69	171
GB1	38	24 Jan 2011	-36.52	-43.38	121	121
GB1	46	26 Jan 2011	-42.21	-41.21	63	100
GB1	59	29 Jan 2011	-51.36	-37.85	60	95
GB1	70	1 Feb 2011	-59.25	-33.15	100	100
GB1	77	3 Feb 2011	-57.28	-25.98	98	100
GB1	85	5 Feb 2011	-53.65	-17.75	73	140
GB1	92	7 Feb 2011	-50.40	-10.80	59	100
GB1	101	9 Feb 2011	-46.31	-3.21	81	140
GB1	109	11 Feb 2011	-42.63	3.34	76	130
GB1	117	13 Feb 2011	-38.97	9.49	62	110
GB2	5	21 Feb 2012	-36.94	39.60	78	90
GB2	27	26 Feb 2012	-45.82	51.05	105	105
GB2	36	28 Feb 2012	-46.84	58.25	90	90
GB2	43	1 Mar 2012	-47.53	64.01	108	125
GB2	53	3 Mar 2012	-49.30	71.32	81	100
GB2	63	5 Mar 2012	-54.40	74.54	109	130
GB2	73	7 Mar 2012	-59.71	77.73	93	75
GB2	87	10 Mar 2012	-54.23	88.22	107	100
GB2	93	11 Mar 2012	-49.81	94.13	113	130
GB2	100	14 Mar 2012	-44.62	100.50	113	90
GB2	106	16 Mar 2012	-40.10	105.34	102	95
GB2	112	17 Mar 2012	-40.26	109.63	76	105
GB2	119	20 Mar 2012	-42.08	113.40	92	90

1711
 1712

1714 Table 2. POC fluxes, concentrations, and attenuation of >51 μm [POC] in the
 1715 mesopelagic zone. Attenuation coefficient is the exponent from significant power law
 1716 fits to >51 μm [POC]. $z_{\text{PAR}}+100\text{m}$ is 100 m below z_{PAR} , as defined in the Table 1
 1717 caption. Transfer efficiency is POC flux at $z_{\text{PAR}}+100\text{m}$ divided by POC flux at z_{PAR} . Deep
 1718 >51 μm [POC] was measured at 1000 m and 800 m for GB1 and GB2, respectively. POC
 1719 flux errors are propagated from ^{234}Th flux, and POC: ^{234}Th errors.

Cruise	Station	Depth	>51 μm [POC] Attenuation Coefficient	^{234}Th Flux at $z_{\text{PAR}}+100\text{m}$	POC:Th at $z_{\text{PAR}}+100\text{m}$	POC Flux at $z_{\text{PAR}}+100\text{m}$	Transfer Efficiency	>51 μm [POC] ($\geq 800\text{m}$)
-	-	<i>m</i>	<i>unitless</i>	<i>dpm m⁻² d⁻¹</i>	$\frac{\mu\text{mol}}{\text{dpm}}$	<i>mmol m⁻² d⁻¹</i>	<i>unitless</i>	μM
GB1	6	179	0.8	3,319 \pm 128 ^c	1.7	5.7 \pm 0.31	1.00	0.030
GB1	16	162	1.1	2,567 \pm 116 ^c	2.4	6.1 \pm 0.30	1.04	No data
GB1	25	162	0.4	1,074 \pm 125	2.5	2.7 \pm 0.37	1.76	0.013
GB1	32	169	0.9	1,581 \pm 186	1.3	2.0 \pm 0.25	0.86	0.006
GB1	38	221	No fit	911 \pm 206	1.6	1.5 \pm 0.35	0.70	0.026
GB1	46	163	1.0	1,937 \pm 146	1.6	3.1 \pm 0.27	0.4	0.009
GB1	59	160	0.6	2,582 \pm 126 ^c	3.7	9.5 \pm 0.56	1.29	0.014
GB1	70	200	0.6	1,414 \pm 248	3.5	5.0 \pm 0.90	0.90	0.024
GB1	77	198	0.5	1,903 \pm 162	2.1	4.0 \pm 0.41	0.44	0.012
GB1	85	173	1.7 ^a	2,076 \pm 207	3.9	8.1 \pm 0.83	0.41	0.035
GB1	92	159	1.1	1,339 \pm 170	3.7	4.9 \pm 0.64	0.61	0.019
GB1	101	181	0.8	1,774 \pm 135	1.7	3.0 \pm 0.24	0.83	0.019
GB1	109	176	1.0	1,719 \pm 97	1.1	1.9 \pm 0.13	0.87	0.006
GB1	117	162	1.1	1,258 \pm 86	1.2	1.5 \pm 0.13	0.87	0.005
GB2	5	178	0.5	1,402 \pm 3,706 ^c	1.1	1.5 \pm 6.1	0.5	No data
GB2	27	205	No fit	2,063 \pm 205	1.2	2.5 \pm 0.30	0.71	No data
GB2	36	190	1.5	1,077 \pm 194	0.9	0.93 \pm 0.18	0.48	0.011
GB2	43	208	1.9	1,247 \pm 200	2.2	2.7 \pm 0.45	0.54	0.005
GB2	53	181	No fit	1,013 \pm 220	2.0	2.0 \pm 0.45	0.49	No data
GB2	63	209	1.8	1,292 \pm 262	1.7	2.1 \pm 0.46	0.31	0.014
GB2	73	193	1.5	807 \pm 189	1.9	1.6 \pm 0.37	0.48	0.008
GB2	87	207	0.7	1,213 \pm 196	1.6	1.9 \pm 0.34	0.60	0.013
GB2	93	213	2.3 ^b	469 \pm 249	1.6	0.77 \pm 0.42	0.53	0.001
GB2	100	213	0.8	1,132 \pm 190	0.7	0.80 \pm 0.15	0.52	0.014
GB2	106	202	0.9	1,405 \pm 186	1.3	1.8 \pm 0.26	1.63	0.017
GB2	112	176	1.3	270 \pm 186	0.9	0.23 \pm 0.21	0.24	0.007
GB2	119	192	No fit	756 \pm 218	0.8	0.57 \pm 0.17	0.20	0.013

1720 ^a attenuation coefficient is 2.35 when only fitting > 51 μm [POC] measurements at depths <500 m (Fig. 3).

1721 ^b outlier approximated by Chauvenet's Theorem (Glover, et al., 2011).

1722 | ^cvalues were estimated by linear interpolation of values at upper and lower depths around $z_{PAR}+100m$.
1723 | “no data”: no measurements at these depths.
1724 | “no fit”: power-law fit was not statistically significant ($p>0.05$).

1725 Table 3. POC, biomineral, and ²³⁴Th concentrations and fluxes at z_{PAR}. EZ- ratio is ²³⁴Th-derived POC flux at z_{PAR} divided by
 1726 integrated primary productivity. The % >51μm [POC] metric is the fraction of total [POC] in the >51 μm size fraction. POC and
 1727 biomineral flux errors are propagated from ²³⁴Th flux, and POC-²³⁴Th errors.

Cruise	Station	z _{PAR}	²³⁴ Th Flux	>51μm [POC]	>51μm [Bsi]	>51μm [PIC]	>51μm Th activity	POC:Th	POC Flux	Bsi:Th	BSi Flux	PIC:Th	PIC Flux	Primary Productivity	Ez- Ratio	% >51 μm [POC]
		m	dpm m ⁻² d ⁻¹	μM	μM	μM	dpm L ⁻¹	μmol dpm ⁻¹	mmol m ⁻² d ⁻¹	μmol dpm ⁻¹	mmol m ⁻² d ⁻¹	μmol dpm ⁻¹	mmol m ⁻² d ⁻¹	mmol m ⁻² d ⁻¹	unitless	%
GB1	6	79	2,437 ± 100	0.23 ^b	0.03 ^a	0.124 ^a	0.07 ^a	2.3 ^a	5.7 ± 0.26	0.4	0.9 ± 0.04	1.8	4.3 ± 0.20	42	0.14	8.8%
GB1	16	62	1,933 ± 71	0.38	0.08	0.390	0.12	3.0	5.9 ± 0.68	0.6	1.2 ± 0.14	3.1	6.1 ± 0.70	165	0.04	17.7%
GB1	25	62	862 ± 46 ^a	0.04	0.005 ^a	0.015 ^a	0.02	1.8	1.6 ± 0.11	0.2	0.2 ± 0.02	0.7	0.6 ± 0.04	35	0.04	3.2%
GB1	32	69	1,304 ± 116	0.07	0.01	0.027	0.04	1.8	2.3 ± 0.21	0.3	0.3 ± 0.03	0.7	0.9 ± 0.08	11	0.21	3.9%
GB1	38	121	809 ± 126	0.04	0.003	0.017	0.01	2.7	2.2 ± 0.35	0.2	0.2 ± 0.03	1.2	0.9 ± 0.15	21	0.10	8.4%
GB1	46	63	2,123 ± 69	0.23	0.005	0.059	0.06	4.1	8.8 ± 0.38	0.1	0.2 ± 0.02	1.1	2.2 ± 0.10	13	0.67	5.3%
GB1	59	60	1,844 ± 102	0.09	0.10	0.072	0.02	4.0	7.3 ± 0.52	4.6	8.6 ± 0.53	3.4	6.2 ± 0.39	26	0.28	5.3%
GB1	70	100	1,280 ± 94	0.11	0.06 ^a	0.001 ^a	0.02	4.3	5.5 ± 0.52	3.5 ^a	4.5 ± 0.53	0.1 ^a	0.1 ± 0.39	10	0.53	10.6%

									0.44	0.35	0.09					
GB1	77	98	1,485 ± 105	0.03	0.03	0.002	0.01	6.0	9.0	5.6	8.3	0.4	0.7	57	0.16	3.6%
									±		±		±			
									1.3		0.98		0.23			
GB1	85	73	1,858 ± 94	2.50	3.44	0.124	0.23	10.8	20	14.9	28	0.5	1.0	53	0.38	52.0%
									±		±		±			
									1.1		1.5		0.05			
GB1	92	59	1,639 ± 77	0.40	0.46	0.020	0.08	4.9	8.0	5.6	9.3	0.2	0.4	26	0.31	11.3%
									±		±		±			
									0.40		0.46		0.02			
GB1	101	81	1,763 ± 82	0.19	0.05	0.013	0.09	2.0	3.6	0.5	0.9	0.1	0.2	22	0.17	12.5%
									±		±		±			
									0.18		0.04		0.01			
GB1	109	76	1,524 ± 76	0.19 ^a	0.05 ^a	0.027 ^a	0.14 ^a	1.4	2.1	0.4	0.6	0.2	0.3	14	0.16	21.0%
									±		±		±			
									0.11		0.03		0.02			
GB1	117	62	1,177 ± 50	0.21	0.02	0.032	0.15	1.4	1.7	0.1	0.2	0.2	0.3	18	0.09	6.6%
									±		±		±			
									0.07		0.01		0.01			
GB2	5	78	1,889 ± 5207	0.08 ^b	0.01 ^a	0.048 ^a	0.05 ^a	1.6	3.0	0.2	0.4	1.0	1.9	8.2	0.37	7.6%
									±		±		±			
									8.8		1.2		5.2			
GB2	27	105	1,869 ± 160	0.08 ^a	0.10 ^a	0.060 ^a	0.04 ^a	1.9	3.5	2.2	4.0	1.3	2.5	8.0	0.44	6.7%
									±		±		±			
									0.32		0.35		0.22			
GB2	36	90	988 ± 89	0.43	0.28	0.074	0.22	2.0	2.0	1.3	1.3	0.3	0.3	12	0.16	15.6%
									±		±		±			
									0.18		0.12		0.03			
GB2	43	108	1,221 ± 153	0.74 ^a	0.62 ^a	0.041 ^a	0.18 ^a	4.1	5.0	3.4	4.2	0.2	0.3	12	0.43	37.8%
									±		±		±			
									0.63		0.53		0.04			
GB2	53	81	1058 ± 100 ^a	0.54 ^a	0.80 ^a	0.081 ^a	0.14 ^a	3.9	4.1	5.7	6.1	0.6	0.6	16	0.25	22.5%
									±		±		±			
									0.40		0.59		0.07			
GB2	63	109	1,229 ± 138	0.71 ^a	1.04 ^a	0.028 ^a	0.13 ^a	5.6 ^a	6.9	8.1	9.9	0.2	0.3	9.0	0.77	33.2%
									±		±		±			
									0.78		1.1		0.03			
GB2	73	93	977 ± 108	0.21 ^b	1.13 ^a	0.014 ^a	0.20 ^a	3.3 ^a	3.2	5.6	5.4	0.1	0.1	8.8	0.36	17.6%
									±		±		±			
									0.36		0.60		0.01			

GB2	87	107	1,299 ± 115	0.06 ^b	0.30 ^a	0.041 ^a	0.06 ^a	2.5 ^a	3.2 ±	4.7	6.1 ±	0.6	0.8 ±	11	0.29	3.4%	
GB2	93	113	1,142 ± 137	0.07 ^a	0.01 ^a	0.023 ^a	0.05 ^a	1.3	0.40 ±	0.2	0.55 ±	0.4	0.5 ±	12	0.12	4.3%	
GB2	100	113	1,112 ± 130	0.08	0.02	0.006	0.06	1.4	0.25 ±	0.3	0.3 ±	0.1	0.1 ±	14	0.11	12.8%	
GB2	106	102	1394 ± 82 ^a	0.09 ^b	0.04 ^a	0.024 ^a	0.12 ^a	0.8	0.19 ±	1.1	0.3 ^a	0.4 ±	0.2	0.3 ±	22	0.05	12.2%
GB2	112	76	717 ± 97	0.22 ^b	0.17 ^a	0.087 ^a	0.36 ^a	1.4 ^a	0.86 ±	1.0	0.5	0.3 ±	0.2	0.2 ±	no data	no data	13.3%
GB2	119	92	1,223 ± 124	0.51 ^a	0.12 ^a	0.048 ^a	0.22 ^a	2.3	0.13 ±	2.8	0.5	0.7 ±	0.2	0.3 ±	17	0.17	21.5%
									0.29		0.07		0.03				

1728
1729
1730
1731
1732
1733

^a values at z_{PAR} estimated by linear interpolation of values at upper and lower depths around z_{PAR} .

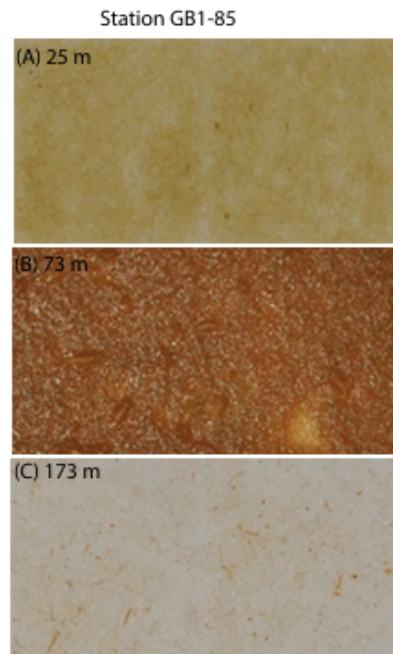
^b >51 μm [POC] values interpolated by significant power-law fits (Fig. 3).

“no data”: not enough depths were sampled and analyzed to interpolate at z_{PAR} .

1734 Table 4. Mean \pm standard deviations of ^{234}Th fluxes, POC: ^{234}Th , BSi: ^{234}Th , PIC: ^{234}Th , POC fluxes, and biomineral fluxes at Z_{PAR} ,
 1735 divided by three latitude zones. 45 °S marks the approximate latitude of the Subantarctic front, while 52 °S marks the approximate
 1736 latitude of the Polar front (Belkin and Gordon, 1996; Sokolov and Rintoul, 2009).
 1737

Lat. zone	^{234}Th Flux at Z_{PAR}	POC:Th at Z_{PAR}	POC Flux at Z_{PAR}	BSi:Th at Z_{PAR}	BSi Flux at Z_{PAR}	PIC:Th at Z_{PAR}	PIC Flux at Z_{PAR}	# stn
°S	$\text{dpm m}^{-2}\text{d}^{-1}$	$\mu\text{mol dpm}^{-1}$	$\text{mmol m}^{-2}\text{d}^{-1}$	$\mu\text{mol dpm}^{-1}$	$\text{mmol m}^{-2}\text{d}^{-1}$	$\mu\text{mol dpm}^{-1}$	$\text{mmol m}^{-2}\text{d}^{-1}$	-
36 - 45	1.3 ± 0.44	1.9 ± 0.9	2.7 ± 2.3	0.3 ± 0.1	0.33 ± 0.17	0.5 ± 0.4	0.73 ± 0.76	10
45 - 52	1.5 ± 0.50	2.8 ± 1.2	4.4 ± 2.2	2.3 ± 2.2	3.4 ± 3.3	1.1 ± 1.2	2.0 ± 2.4	11
52 - >60	1.4 ± 0.30	5.4 ± 3.0	8.0 ± 6.3	7.1 ± 4.1	10 ± 8.7	0.3 ± 0.2	0.49 ± 0.4	6

1738 Figure 1. Cruise tracks across the Atlantic (cruise GB1) and Indian (cruise GB2) sectors
1739 of the Great Calcite Belt showing sea surface temperature along the two transects. Station
1740 numbers where only ^{234}Th and size-fractionated particles were sampled are indicated by
1741 crosses. The two horizontal dashed lines at 45 °S and 52 °S represent the approximate
1742 locations of the Subantarctic and Polar fronts, respectively (Belkin and Gordon, 1996;
1743 Sokolov and Rintoul, 2009).



1744
1745 Figure 2. Digital images of $>51\ \mu\text{m}$ filters from station GB1-85 (refer to Fig. 1 for station
1746 location). $>51\ \mu\text{m}$ particles are from (a) 25m in the euphotic zone, (b) 73m, which
1747 corresponds to z_{PAR} , as defined in Table 1, and (c) at 173m, below both metrics of export
1748 depth, z_{PAR} and $z_{\text{TH/U}}$ (Table 1). $>51\ \mu\text{m}$ particles in the euphotic zone appear as dense
1749 sheets of intact cells packed onto the filters (a, b) and as more sparsely arranged
1750 cylindrical fecal pellets on filters collected below z_{PAR} (c).

1751
1752 Figure 3. Significant power law fits of $>51\ \mu\text{m}$ [POC] below z_{PAR} , according to Eq. (1).
1753 Only the 22 significant fits are shown as lines. Three stations are highlighted to show the
1754 range in $>51\ \mu\text{m}$ [POC] attenuation across GB1 and GB2 profiles (symbols represent

Sarah Rosengard 5/19/15 11:27 AM
Deleted: in the euphotic zone

1756 measurements): GB1-85 had the highest POC concentration through the water column
1757 and an attenuation coefficient of 1.7; GB1-25 had the lowest attenuation coefficient (0.4);
1758 GB2-43 had the highest attenuation coefficient (1.9) (Table 2). Fitting GB1-85 $>51 \mu\text{m}$
1759 [POC] measurements between z_{PAR} and 500 m yields a higher attenuation coefficient of
1760 2.35. Refer to Fig. 1 for station locations.

1761

1762 Figure 4. Total ^{234}Th and ^{238}U activity profiles measured at 14 stations of GB1 and 13
1763 stations of GB2 (note different x-axis for station GB2-5) (Table S1). Error bars for ^{234}Th
1764 activity are propagated errors. ^{238}U is calculated from salinity. All ^{234}Th activity profiles
1765 exhibit a deficit relative to ^{238}U activity at the surface, and mostly return to equilibrium
1766 with ^{234}U within error at depth of $z_{\text{Th/U}}$ (Table 1). Refer to Fig. 1 for station locations.

1767

1768 Figure 5. Distribution of ^{234}Th flux and ^{234}Th -derived POC flux at 27 stations along GB1
1769 and GB2 (circle area scales with flux magnitude). (a) ^{234}Th fluxes at z_{PAR} range from 717
1770 $\text{dpm m}^{-2} \text{d}^{-1}$ to 2,437 $\text{dpm m}^{-2} \text{d}^{-1}$ at stations GB2-112 and GB1-6, respectively. (b) POC
1771 fluxes at z_{PAR} range from 0.97 $\text{mmol m}^{-2} \text{d}^{-1}$ to 20 $\text{mmol m}^{-2} \text{d}^{-1}$ at stations GB2-112 and
1772 GB1-85, respectively. (c) POC fluxes at $z_{\text{Th/U}}$ range from 0.57 to 12 $\text{mmol m}^{-2} \text{d}^{-1}$ at
1773 stations GB2-112 and GB1-85, respectively (Table S2). (d) POC fluxes at 100m below
1774 z_{PAR} range from 0.23 to 9.5 $\text{mmol m}^{-2} \text{d}^{-1}$ at stations GB2-112 and GB1-59, respectively.
1775 A few station numbers discussed in the text are indicated. Red outlines distinguish
1776 stations where fluxes are greater at the specified depth than at z_{PAR} . The two horizontal
1777 dashed lines at 45 °S and 52 °S represent the approximate locations of the Subantarctic
1778 and Polar fronts, respectively (Belkin and Gordon, 1996; Sokolov and Rintoul, 2009).
1779 Refer to Fig. 1 for other station locations. z_{PAR} and $z_{\text{Th/U}}$ are defined as in Table 1.

1780

1781 Figure 6. Distribution of BSi flux, PIC flux, and % $>51 \mu\text{m}$ [POC], the percent of total
1782 [POC] in the $>51 \mu\text{m}$ size class, at z_{PAR} (Table 1) along GB1 and GB2 (circle area scales
1783 with magnitude). (a) BSi fluxes range from 0.17 $\text{mmol m}^{-2} \text{d}^{-1}$ to 28 $\text{mmol m}^{-2} \text{d}^{-1}$ at
1784 stations GB1-46 and GB1-85, respectively. (b) PIC fluxes range from 0.067 to 6.2 mmol
1785 $\text{m}^{-2} \text{d}^{-1}$ at stations GB2-73 and GB2-59, respectively. (c) The proportion of [POC] in the
1786 $>51 \mu\text{m}$ size-fraction at z_{PAR} ranges from 3.3% to 52% at stations GB1-25 and GB1-85,

1787 respectively. A few station numbers discussed in the text are indicated. The two
1788 horizontal dashed lines at 45 °S and 52 °S represent the approximate locations of the
1789 Subantarctic and Polar fronts, respectively (Belkin and Gordon, 1996; Sokolov and
1790 Rintoul, 2009). Refer to Fig. 1 for other station locations.

1791
1792 Figure 7. Distribution of primary productivity, export efficiency, and transfer efficiency
1793 along GB1 and GB2 (circle area scales with magnitude). (a) Primary productivity
1794 integrated through the euphotic zone ranges from 8.0 to 165 mmol m⁻² d⁻¹ at stations
1795 GB2-27 and GB1-16, respectively. (b) Export efficiency (EZ-ratio) at z_{PAR} (Table 1),
1796 which is the ratio of ²³⁴Th-derived POC flux at z_{PAR} to primary productivity integrated to
1797 z_{PAR}, ranges from 0.04 to 0.77 at stations GB1-16 and GB2-63, respectively. (c) Transfer
1798 efficiency at z_{PAR}, which is the ratio of POC flux 100 m below z_{PAR} to POC flux at z_{PAR},
1799 ranges from 0.20 to 1.8 at stations GB1-119 and GB1-25, respectively. A few station
1800 numbers discussed in the text are indicated. The two horizontal dashed lines at 45 °S and
1801 52 °S represent the approximate locations of the Subantarctic and Polar fronts,
1802 respectively (Belkin and Gordon, 1996; Sokolov and Rintoul, 2009). Refer to Fig. 1 for
1803 other station locations.

1804
1805 Figure 8. Distribution and vertical attenuation coefficient of >51 μm [POC] (circle area
1806 scales with magnitude). (a) >51 μm POC concentrations at z_{PAR} (Table 1) range from
1807 0.03 μM to 2.5 μM at stations GB1-77 and GB1-85, respectively. (b) >51 μm [POC] at
1808 the deepest pump depth in the lower mesopelagic zone (800 m-1000 m). Concentrations
1809 range from 0.001 μM to 0.035 μM at stations GB2-93 and GB1-85, respectively. (c)
1810 Attenuation coefficient from significant power-law fits of 22 >51 μm [POC] profiles,
1811 excluding GB2-93 (see Sect. 4.4). A few station numbers discussed in the text are
1812 indicated. The two horizontal dashed lines at 45 °S and 52 °S represent the approximate
1813 locations of the Subantarctic and Polar fronts, respectively (Belkin and Gordon, 1996;
1814 Sokolov and Rintoul, 2009). Refer to Fig. 1 for other station locations.

1815
1816 Figure 9. ²³⁴Th-derived POC flux as a function of (a) PIC flux and (b) BSi flux at z_{PAR}.
1817 POC flux transfer efficiency between z_{PAR} and z_{PAR}+100 m (T₁₀₀, defined in Sect. 4.4) as

1818 a function of (c) PIC flux and (d) BSi flux at z_{PAR} . Significant linear relationships are
1819 plotted as a solid blue line. T_{100} values at GB1-25 and GB2-106 were excluded from all
1820 correlations (Sect. 4.4). Color_{bar} indicates longitude of stations— GB1 and GB2 stations
1821 are in cool and warm colors, respectively. Refer to Fig. 1 for more specific station
1822 locations.

1823

1824 Figure 10. Attenuation coefficient as a function of (a) $>51 \mu\text{m}$ [BSi] at z_{PAR} and (b) the
1825 proportion of [POC] in the $>51 \mu\text{m}$ size-fraction at z_{PAR} . The open circle indicates where
1826 GB1-85 would plot with a higher attenuation coefficient of 2.35, derived from fitting >51
1827 μm [POC] at depths between z_{PAR} and 500 m. Significant linear relationships using the
1828 lower and higher attenuation coefficient values for GB1-85 are shown as solid and
1829 dashed lines, respectively; p and r^2 values are provided for the solid lines. The color_{bar} is
1830 the natural logarithm of the ratio of $>51 \mu\text{m}$ PIC:BSi at z_{PAR} . We interpret all warm

1831 colors >0 to indicate stations with a high relative abundance of coccolithophores, and all
1832 cool values <0 to indicate stations with a high relative abundance of diatoms (Figs. S2,
1833 S3). A few station numbers discussed in the text are indicated. Refer to Fig. 1 for station
1834 locations.

Sarah Rosengard 5/20/15 5:54 PM

Deleted: -dominated

Sarah Rosengard 5/20/15 5:54 PM

Deleted: stations

Sarah Rosengard 5/20/15 5:54 PM

Deleted: -dominated stations

Supplement Contents

This supplement contains, in the following order:

Table S1: tabulated ^{234}Th activity, ^{234}U activity and ^{234}Th flux profiles

Table S2: tabulated ^{234}Th and POC fluxes and POC: ^{234}Th ratios at $z_{\text{Th/U}}$

Figure S1. Plotted profiles of POC: ^{234}Th , PIC: ^{234}Th and BSi: ^{234}Th above 400 m

Figure S2. Euphotic zone diatom or coccolithophore abundance as a function of [BSi] or [PIC], respectively

Figure S3: The natural log ratio of [PIC] to [BSi] as a function of the natural log ratio of total euphotic zone coccolithophore to diatom abundances

Figure S4: Percentage of total cell counts that are diatoms at z_{PAR} as a function of the in-situ pump size fractionation of [POC] at z_{PAR}

Supplementary Methods: pertaining to data from Figures S2-S4.

Supplementary References

Table S1. ^{234}Th activity and flux profiles estimated at 27 stations along cruises GB1 and GB2. Fluxes were estimated by measuring total seawater ^{234}Th activity deficits relative to total seawater ^{238}U activity, as described in Sect. 2.4. ^{234}Th flux errors are propagated from ^{234}Th activity errors.

Cruise	Station	Depth	^{234}Th Activity	^{234}Th Activity Error	^{238}U Activity	^{234}Th Flux	^{234}Th Flux Error
-	-	<i>m</i>	<i>dpm L⁻¹</i>	<i>dpm L⁻¹</i>	<i>dpm L⁻¹</i>	<i>dpm m⁻² d⁻¹</i>	<i>dpm m⁻² d⁻¹</i>
GB1	6	13.6	1.04	0.02	2.36	681	27
GB1	6	22.3	1.28	0.05	2.36	924	31
GB1	6	29.2	1.12	0.03	2.36	1,243	34
GB1	6	40.2	1.23	0.03	2.36	1,503	37
GB1	6	45.2	1.29	0.06	2.36	1,702	39
GB1	6	53.1	1.53	0.04	2.36	2,096	48
GB1	6	78	1.86	0.12	2.36	2,437	100
GB1	6	100.6	1.90	0.05	2.36	2,684	106
GB1	6	115	2.08	0.10	2.36	2,804	116
GB1	6	130	2.15	0.05	2.36	2,911	121
GB1	6	150.3	2.09	0.07	2.36	3,182	145
GB1	6	200	2.04	0.18	2.37	3,419	195
GB1	16	11.1	0.99	0.02	2.35	548	20
GB1	16	17.07	1.10	0.02	2.35	762	22
GB1	16	23.04	0.94	0.02	2.35	1,107	25
GB1	16	34.2	1.61	0.04	2.35	1,311	30
GB1	16	42.2	1.61	0.05	2.36	1,611	42
GB1	16	62.3	1.97	0.05	2.36	1,933	71
GB1	16	100.17	2.06	0.05	2.36	2,277	105
GB1	16	140.8	2.18	0.06	2.37	2,487	139
GB1	16	180.1	2.24	0.08	2.37	2,636	178
GB1	16	220.5	2.21	0.21	2.37	2,819	308
GB1	16	260.7	2.37	0.13	2.37	2,810	394
GB1	16	340.3	2.16	0.08	2.37	3,040	409
GB1	25	10.3	1.70	0.05	2.45	283	26
GB1	25	16.1	1.95	0.06	2.45	380	30
GB1	25	23.8	1.91	0.03	2.45	525	34
GB1	25	34.5	2.14	0.05	2.47	611	38
GB1	25	41.7	2.07	0.07	2.47	773	51
GB1	25	80	2.42	0.03	2.48	941	74
GB1	25	115	2.46	0.04	2.45	937	91
GB1	25	140.5	2.38	0.05	2.43	975	103
GB1	25	165.2	2.32	0.07	2.44	1,074	125
GB1	25	200.2	2.44	0.04	2.42	1,029	177

GB1	25	300	2.36	0.03	2.38	1,051	195
GB1	32	12.15	1.96	0.08	2.48	229	41
GB1	32	18	1.96	0.06	2.48	327	44
GB1	32	25.25	2.00	0.07	2.49	475	51
GB1	32	39.2	2.02	0.10	2.49	614	61
GB1	32	46	2.05	0.19	2.49	808	104
GB1	32	69.67	1.83	0.04	2.47	1,304	116
GB1	32	100.2	2.33	0.03	2.48	1,435	127
GB1	32	130.5	2.38	0.03	2.47	1,520	141
GB1	32	171	2.41	0.09	2.46	1,581	186
GB1	32	210	2.43	0.03	2.46	1,612	198
GB1	32	251	2.29	0.11	2.45	1,818	250
GB1	32	300.8	2.52	0.03	2.44	1,761	253
GB1	38	20.4	2.36	0.08	2.52	127	72
GB1	38	32.2	2.17	0.03	2.52	247	74
GB1	38	44.2	2.20	0.04	2.52	418	83
GB1	38	69	2.28	0.10	2.53	550	102
GB1	38	81	2.27	0.08	2.54	638	107
GB1	38	92	2.34	0.03	2.53	743	113
GB1	38	121	2.43	0.05	2.51	809	126
GB1	38	150	2.41	0.09	2.50	886	151
GB1	38	175	2.57	0.05	2.50	811	168
GB1	38	220	2.43	0.06	2.50	911	206
GB1	38	280.2	2.47	0.05	2.48	938	247
GB1	38	350.7	2.74	0.08	2.48	678	265
GB1	46	10	1.40	0.02	2.43	395	20
GB1	46	16.8	1.47	0.03	2.43	573	23
GB1	46	23	1.54	0.03	2.43	813	28
GB1	46	35.7	1.41	0.02	2.42	1,090	32
GB1	46	42.03	1.37	0.02	2.42	1,338	34
GB1	46	52.1	1.36	0.03	2.42	1,652	38
GB1	46	62.7	1.74	0.07	2.42	2,123	69
GB1	46	100.4	2.44	0.03	2.41	2,089	102
GB1	46	150.4	2.51	0.05	2.40	1,937	146
GB1	46	200.4	2.46	0.05	2.40	1,850	174
GB1	46	250.2	2.37	0.11	2.39	1,874	283
GB1	46	325.3	2.53	0.12	2.38	1,712	314
GB1	59	10.4	1.46	0.03	2.34	335	21
GB1	59	16.1	1.43	0.06	2.34	493	25
GB1	59	22.5	1.64	0.21	2.34	673	61
GB1	59	34	1.61	0.12	2.34	857	69
GB1	59	40	1.50	0.03	2.34	1,013	70
GB1	59	47	1.49	0.05	2.34	1,256	73

GB1	59	60	1.49	0.09	2.34	1,844	102
GB1	59	95	2.12	0.05	2.35	2,108	128
GB1	59	140	2.05	0.06	2.36	2,509	159
GB1	59	185	2.24	0.09	2.37	2,673	202
GB1	59	225	2.16	0.05	2.37	3,113	244
GB1	59	325	2.34	0.04	2.40	3,189	262
GB1	70	17	1.86	0.06	2.36	314	47
GB1	70	27	1.85	0.06	2.36	460	52
GB1	70	37	1.76	0.05	2.36	721	61
GB1	70	57.5	1.81	0.06	2.36	967	69
GB1	70	68	1.90	0.05	2.37	1,119	72
GB1	70	80	2.05	0.05	2.37	1,266	80
GB1	70	100	2.36	0.06	2.38	1,280	94
GB1	70	125	2.29	0.18	2.38	1,361	190
GB1	70	160	2.35	0.06	2.39	1,412	208
GB1	70	200	2.40	0.09	2.40	1,414	248
GB1	70	250	2.45	0.09	2.40	1,342	286
GB1	70	300	2.27	0.06	2.41	1,439	292
GB1	77	17	1.71	0.06	2.35	399	45
GB1	77	26	1.68	0.05	2.35	573	49
GB1	77	35	1.84	0.05	2.35	794	57
GB1	77	56	1.79	0.06	2.35	1,047	66
GB1	77	66	1.86	0.06	2.35	1,197	70
GB1	77	77	1.97	0.06	2.36	1,391	79
GB1	77	101	2.25	0.08	2.37	1,485	105
GB1	77	130	2.30	0.06	2.39	1,561	122
GB1	77	160	2.31	0.06	2.39	1,630	139
GB1	77	190	2.16	0.05	2.40	1,903	162
GB1	77	240	2.40	0.07	2.40	1,917	213
GB1	77	300	2.40	0.13	2.41	1,922	243
GB1	85	12.6	1.30	0.05	2.35	476	32
GB1	85	19	1.55	0.07	2.35	629	35
GB1	85	26	1.41	0.06	2.35	925	43
GB1	85	41	1.52	0.07	2.35	1,197	52
GB1	85	49	1.76	0.07	2.35	1,340	56
GB1	85	58	1.91	0.07	2.35	1,493	63
GB1	85	73	1.86	0.08	2.35	1,858	94
GB1	85	110	2.17	0.09	2.36	2,034	133
GB1	85	140	2.34	0.09	2.36	2,059	168
GB1	85	180	2.36	0.09	2.37	2,076	207
GB1	85	220	2.46	0.09	2.38	1,931	273
GB1	85	300	2.60	0.10	2.39	1,683	300
GB1	92	10	1.68	0.07	2.34	239	32

GB1	92	15	1.61	0.07	2.34	365	35
GB1	92	22	1.54	0.07	2.34	571	41
GB1	92	33	1.78	0.04	2.34	709	43
GB1	92	39	1.65	0.05	2.34	837	45
GB1	92	46	1.59	0.04	2.34	1,053	48
GB1	92	59	1.59	0.06	2.34	1,639	77
GB1	92	100	2.65	0.07	2.35	1,332	117
GB1	92	130	2.28	0.06	2.36	1,396	134
GB1	92	160	2.41	0.09	2.36	1,339	170
GB1	92	200	2.42	0.06	2.37	1,248	232
GB1	92	302	2.29	0.06	2.38	1,391	259
GB1	101	13.6	1.57	0.04	2.36	405	33
GB1	101	22	1.46	0.04	2.36	611	35
GB1	101	29.5	1.58	0.05	2.36	867	42
GB1	101	45	1.61	0.05	2.36	1,133	49
GB1	101	54	1.74	0.06	2.37	1,296	52
GB1	101	63	1.89	0.06	2.37	1,484	61
GB1	101	81	1.96	0.07	2.37	1,763	82
GB1	101	110	2.24	0.07	2.38	1,878	107
GB1	101	140	2.43	0.05	2.37	1,826	122
GB1	101	171	2.43	0.05	2.37	1,774	135
GB1	101	200	2.44	0.05	2.37	1,641	184
GB1	101	300	2.20	0.04	2.37	1,883	205
GB1	109	11.1	1.58	0.03	2.39	318	23
GB1	109	16.2	1.69	0.04	2.39	445	25
GB1	109	23.7	1.62	0.04	2.39	672	31
GB1	109	36.5	1.77	0.04	2.40	854	35
GB1	109	44	1.76	0.04	2.48	1,158	44
GB1	109	66	2.03	0.04	2.40	1,326	53
GB1	109	76	1.99	0.04	2.40	1,524	61
GB1	109	100	2.17	0.04	2.39	1,648	71
GB1	109	115	2.19	0.04	2.40	1,737	76
GB1	109	130	2.43	0.05	2.40	1,722	83
GB1	109	150	2.40	0.05	2.40	1,719	94
GB1	109	175	2.40	0.05	2.40	1,719	97
GB1	117	10.5	1.80	0.04	2.43	243	24
GB1	117	16.3	1.69	0.03	2.43	377	26
GB1	117	23	1.99	0.04	2.43	484	30
GB1	117	33	1.77	0.04	2.41	659	34
GB1	117	42	1.95	0.04	2.41	758	37
GB1	117	48	1.86	0.04	2.42	918	41
GB1	117	62	1.87	0.04	2.43	1,177	50
GB1	117	80	2.08	0.04	2.44	1,346	58

GB1	117	95	2.31	0.05	2.44	1,404	65
GB1	117	110	2.46	0.05	2.44	1,394	71
GB1	117	125	2.61	0.05	2.43	1,290	82
GB1	117	150	2.52	0.05	2.43	1,258	86
GB2	5	20	1.37	6.03	2.47	948	5,206
GB2	5	40	1.70	0.08	2.47	1,403	5,206
GB2	5	61	1.84	0.07	2.47	1,768	5,206
GB2	5	71	1.89	0.15	2.48	2,015	5,206
GB2	5	80	2.18	0.07	2.47	1,889	5,207
GB2	5	90	2.56	0.07	2.47	1,862	5,207
GB2	5	100	2.52	0.08	2.48	1,850	5,207
GB2	5	111	2.54	0.08	2.47	1,832	5,207
GB2	5	120	2.44	0.09	2.47	1,849	5,207
GB2	5	150	2.50	0.07	2.48	1,821	5,208
GB2	5	201	2.82	0.14	2.47	1,058	5,218
GB2	5	300	2.71	0.09	2.46	695	5,220
GB2	27	20	1.70	0.04	2.34	554	53
GB2	27	40	1.56	0.04	2.34	1,114	69
GB2	27	70	1.68	0.06	2.34	1,637	92
GB2	27	85	1.53	0.24	2.34	2,047	155
GB2	27	95	1.97	0.05	2.34	1,828	159
GB2	27	105	2.20	0.06	2.35	1,869	160
GB2	27	115	2.21	0.08	2.35	1,910	162
GB2	27	125	2.28	0.06	2.35	1,931	164
GB2	27	135	2.27	0.05	2.35	1,972	168
GB2	27	160	2.18	0.06	2.35	2,130	181
GB2	27	200	2.41	0.06	2.36	2,063	205
GB2	27	250	2.69	0.08	2.36	1,826	216
GB2	36	20	1.83	0.04	2.34	434	55
GB2	36	40	1.86	0.06	2.34	639	65
GB2	36	50	1.82	0.08	2.34	824	73
GB2	36	65	1.91	0.05	2.34	981	77
GB2	36	75	2.19	0.08	2.35	1,035	84
GB2	36	90	2.48	0.06	2.35	988	89
GB2	36	100	2.29	0.08	2.35	1,034	117
GB2	36	125	2.04	0.07	2.35	1,372	148
GB2	36	150	2.23	0.06	2.35	1,161	169
GB2	36	175	2.42	0.06	2.35	1,110	178
GB2	36	200	2.39	0.05	2.36	1,077	194
GB2	36	250	2.58	0.07	2.36	923	202
GB2	43	20	1.89	0.04	2.33	383	55
GB2	43	40	1.90	0.08	2.33	632	76
GB2	43	60	1.93	0.08	2.33	896	99

GB2	43	85	2.06	0.07	2.34	1,034	108
GB2	43	95	2.03	0.05	2.34	1,147	111
GB2	43	110	2.17	0.24	2.34	1,221	153
GB2	43	125	2.25	0.05	2.34	1,258	156
GB2	43	140	2.25	0.10	2.34	1,308	169
GB2	43	165	2.45	0.06	2.34	1,233	177
GB2	43	190	2.35	0.06	2.35	1,230	186
GB2	43	220	2.33	0.07	2.35	1,247	200
GB2	43	250	2.68	0.09	2.36	1,108	205
GB2	53	20	1.87	0.08	2.34	407	80
GB2	53	40	1.88	0.14	2.34	668	117
GB2	53	60	1.99	0.05	2.34	915	126
GB2	53	90	1.98	0.05	2.34	1,120	132
GB2	53	100	2.27	0.08	2.34	1,139	134
GB2	53	110	2.45	0.06	2.34	1,109	136
GB2	53	120	2.40	0.06	2.34	1,056	151
GB2	53	170	2.38	0.11	2.35	1,013	220
GB2	53	210	2.52	0.06	2.35	827	237
GB2	53	250	2.30	0.06	2.36	860	241
GB2	63	20	1.88	0.09	2.34	394	88
GB2	63	40	1.94	0.08	2.34	625	102
GB2	63	60	1.95	0.08	2.34	848	115
GB2	63	80	1.92	0.05	2.34	1,089	121
GB2	63	100	2.12	0.13	2.34	1,187	135
GB2	63	110	2.20	0.08	2.34	1,229	138
GB2	63	120	2.25	0.10	2.34	1,285	151
GB2	63	130	2.31	0.10	2.34	1,316	174
GB2	63	150	2.37	0.09	2.35	1,267	191
GB2	63	175	2.38	0.09	2.35	1,248	204
GB2	63	200	2.32	0.14	2.36	1,292	262
GB2	63	250	2.50	0.09	2.37	1,198	272
GB2	73	20	1.80	0.06	2.35	433	63
GB2	73	35	1.79	0.06	2.35	675	71
GB2	73	50	1.94	0.09	2.35	823	79
GB2	73	60	1.96	0.07	2.35	966	85
GB2	73	75	2.30	0.11	2.37	997	99
GB2	73	90	2.43	0.09	2.38	977	108
GB2	73	105	2.63	0.07	2.39	822	120
GB2	73	120	2.58	0.12	2.39	677	156
GB2	73	135	2.43	0.06	2.40	794	168
GB2	73	160	2.34	0.06	2.40	853	184
GB2	73	200	2.48	0.06	2.40	807	189
GB2	87	20	1.93	0.07	2.35	354	71

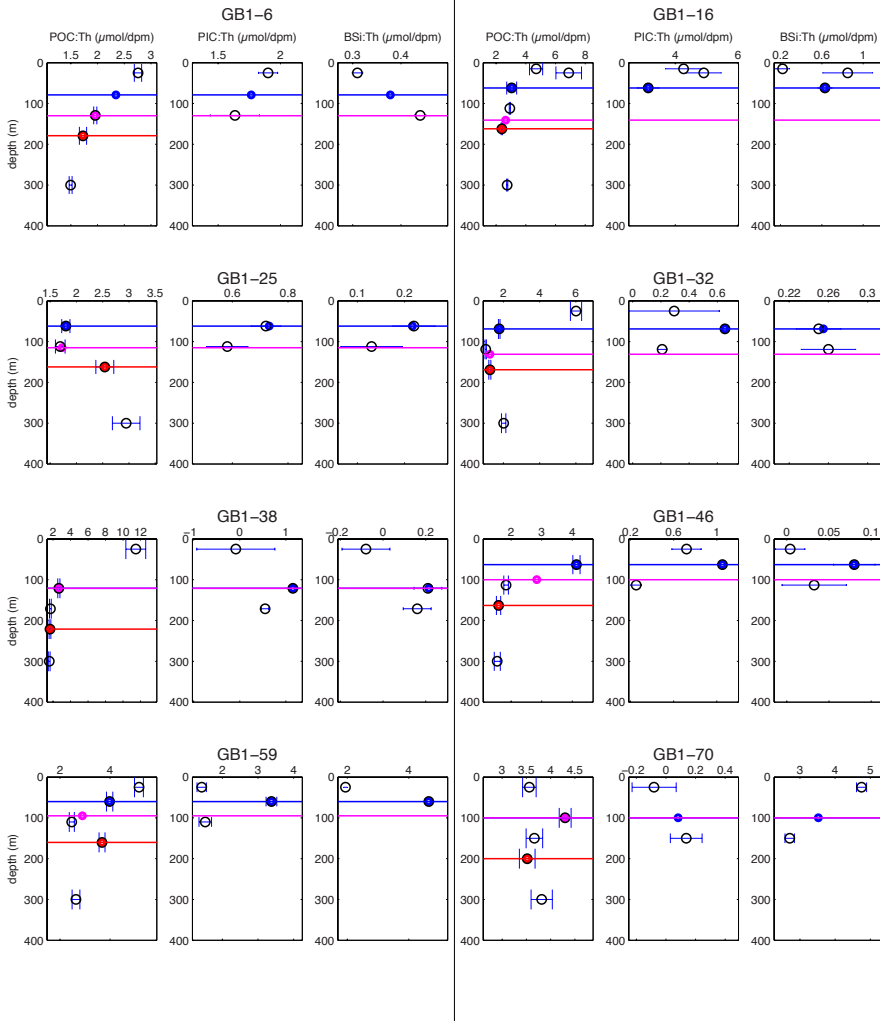
GB2	87	40	1.92	0.05	2.35	599	81
GB2	87	60	1.75	0.06	2.35	939	91
GB2	87	80	1.89	0.07	2.35	1,134	98
GB2	87	90	1.88	0.05	2.35	1,268	100
GB2	87	100	2.28	0.08	2.35	1,290	103
GB2	87	110	2.33	0.13	2.35	1,299	115
GB2	87	125	2.35	0.08	2.36	1,302	121
GB2	87	140	2.36	0.08	2.36	1,297	136
GB2	87	170	2.32	0.08	2.36	1,336	159
GB2	87	200	2.48	0.09	2.37	1,213	196
GB2	87	250	2.55	0.08	2.38	1,088	208
GB2	93	20	1.95	0.07	2.36	352	71
GB2	93	40	2.04	0.09	2.36	554	96
GB2	93	65	2.14	0.08	2.36	710	116
GB2	93	90	1.95	0.08	2.36	944	127
GB2	93	105	2.01	0.08	2.36	1,071	132
GB2	93	115	2.17	0.10	2.37	1,142	137
GB2	93	130	2.57	0.09	2.39	1,061	144
GB2	93	145	2.44	0.08	2.39	1,033	152
GB2	93	165	2.42	0.08	2.39	1,003	170
GB2	93	180	2.40	0.09	2.39	992	213
GB2	93	200	2.82	0.09	2.39	469	249
GB2	93	250	2.61	0.09	2.38	309	259
GB2	100	20	1.89	0.05	2.42	464	58
GB2	100	40	1.90	0.07	2.42	764	75
GB2	100	60	2.06	0.07	2.42	922	83
GB2	100	70	1.80	0.05	2.42	1,101	85
GB2	100	80	2.27	0.08	2.43	1,145	89
GB2	100	90	2.33	0.08	2.43	1,174	94
GB2	100	100	2.66	0.28	2.43	1,110	124
GB2	100	110	2.43	0.08	2.43	1,112	130
GB2	100	130	2.30	0.09	2.43	1,205	151
GB2	100	160	2.48	0.09	2.43	1,157	182
GB2	100	200	2.47	0.08	2.43	1,132	190
GB2	106	20	1.87	0.05	2.47	603	68
GB2	106	50	1.77	0.05	2.47	1,005	79
GB2	106	60	1.83	0.06	2.47	1,189	82
GB2	106	70	2.09	0.08	2.48	1,301	86
GB2	106	80	2.17	0.08	2.48	1,413	92
GB2	106	95	2.45	0.09	2.48	1,426	107
GB2	106	115	2.62	0.09	2.48	1,335	126
GB2	106	140	2.50	0.06	2.48	1,320	138
GB2	106	165	2.36	0.06	2.48	1,423	154

GB2	106	200	2.49	0.07	2.47	1,405	186
GB2	106	250	2.64	0.17	2.46	1,274	226
GB2	112	10	2.11	0.08	2.42	136	40
GB2	112	20	2.39	0.09	2.42	149	54
GB2	112	35	2.29	0.08	2.42	199	65
GB2	112	45	1.91	0.07	2.43	347	69
GB2	112	55	1.80	0.07	2.42	526	73
GB2	112	65	2.25	0.09	2.42	589	82
GB2	112	80	2.20	0.08	2.43	717	97
GB2	112	105	2.47	0.09	2.43	682	126
GB2	112	135	2.66	0.09	2.42	466	160
GB2	112	170	2.63	0.09	2.42	270	186
GB2	112	200	2.69	0.10	2.42	-39	223
GB2	112	250	2.66	0.10	2.42	-211	237
GB2	119	10	1.73	0.19	2.42	347	96
GB2	119	25	1.73	0.05	2.42	644	101
GB2	119	40	1.77	0.06	2.42	923	106
GB2	119	55	2.00	0.07	2.42	1,072	110
GB2	119	65	2.16	0.07	2.43	1,147	113
GB2	119	74	2.21	0.07	2.43	1,226	117
GB2	119	90	2.43	0.08	2.43	1,223	124
GB2	119	105	2.32	0.08	2.42	1,280	135
GB2	119	130	2.60	0.08	2.43	1,127	158
GB2	119	165	2.69	0.09	2.42	853	189
GB2	119	200	2.50	0.08	2.42	756	218
GB2	119	250	2.75	0.09	2.42	516	231

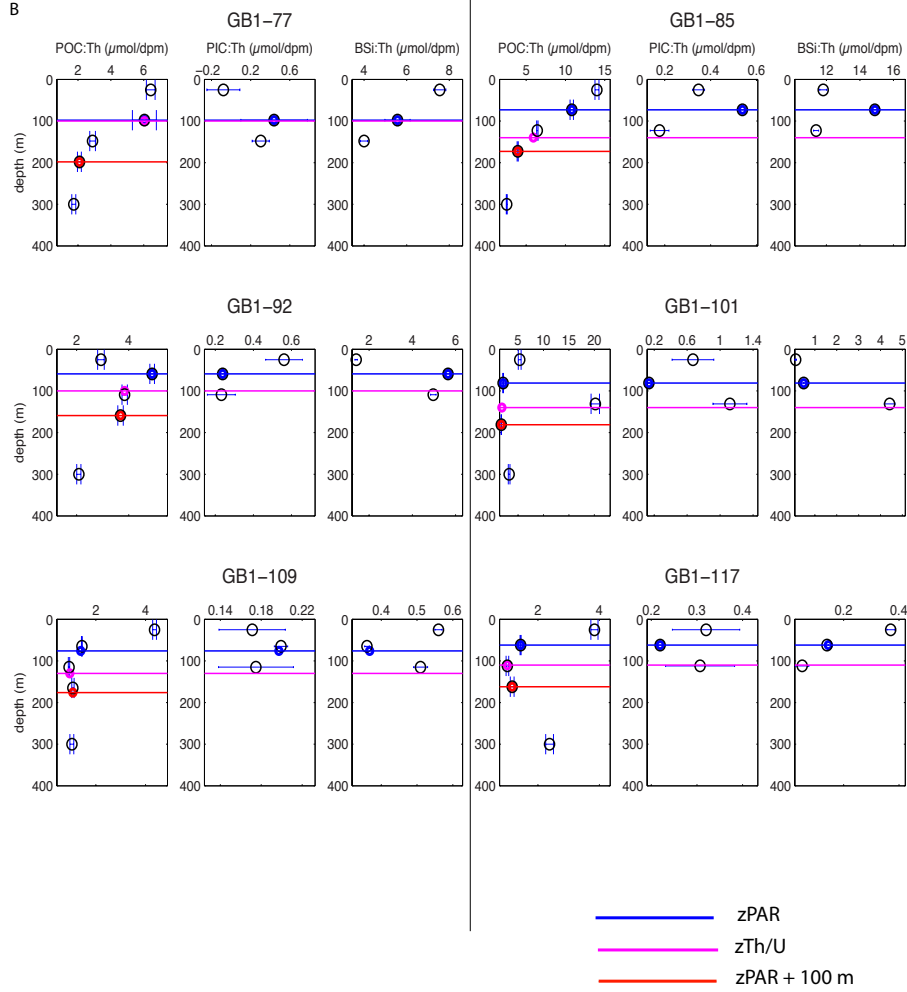
Table S2. ^{234}Th and POC fluxes at $z_{\text{Th/U}}$, estimated at 27 stations along cruises GB1 and GB2. $z_{\text{Th/U}}$ is the depth where ^{234}Th and ^{238}U activities re-establish secular equilibrium. Calculations of POC flux from ^{234}Th fluxes are described in Sect. 2.4. POC flux errors are propagated from ^{234}Th flux, and POC: ^{234}Th errors.

Cruise	Station	$z_{\text{Th/U}}$	^{234}Th Flux	^{234}Th Flux Error	$>51\mu\text{m POC} : ^{234}\text{Th}$	POC Flux	POC Flux Error
-	-	<i>m</i>	<i>dpm m⁻² d⁻¹</i>	<i>dpm m⁻² d⁻¹</i>	<i>μmol dpm⁻¹</i>	<i>mmol m⁻² d⁻¹</i>	<i>mmol m⁻² d⁻¹</i>
GB1	6	130	2,911	121	2.0	5.7	0.25
GB1	16	140.8	2,487	139	2.6	6.6	0.37
GB1	25	115	937	91	1.7	1.6	0.18
GB1	32	131	1,581	186	1.3	2.0	0.20
GB1	38	121	809	126	2.7	2.2	0.35
GB1	46	100	2,089	102	2.8	5.9	0.32
GB1	59	95	2,108	128	2.9	6.1	0.42
GB1	70	100	1,280	94	4.3	5.5	0.44
GB1	77	100	1,485	105	6.0	9.0	1.3
GB1	85	140	2,059	168	5.9	12	1.0
GB1	92	100	1,332	117	3.8	5.1	0.47
GB1	101	140	1,826	122	1.8	3.3	0.23
GB1	109	130	1,722	83	1.0	1.6	0.09
GB1	117	110	1,394	71	1.0	1.4	0.09
GB2	5	90	1,862	5,207	1.3	2.5	6.9
GB2	27	105	1,869	160	1.9	3.5	0.32
GB2	36	90	988	89	2.0	2.0	0.18
GB2	43	125	1,258	156	3.7	4.6	0.58
GB2	53	100	1,139	134	3.9	4.4	0.53
GB2	63	130	1,316	174	4.6	6.1	0.81
GB2	73	75	997	99	4.9	4.9	0.49
GB2	87	100	1,290	103	2.9	3.8	0.33
GB2	93	130	1,061	144	1.2	1.2	0.18
GB2	100	90	1,174	94	2.8	3.3	0.27
GB2	106	95	1,426	107	0.9	1.2	0.10
GB2	112	105	682	126	0.8	0.6	0.11
GB2	119	90	1,223	124	2.5	3.0	0.31

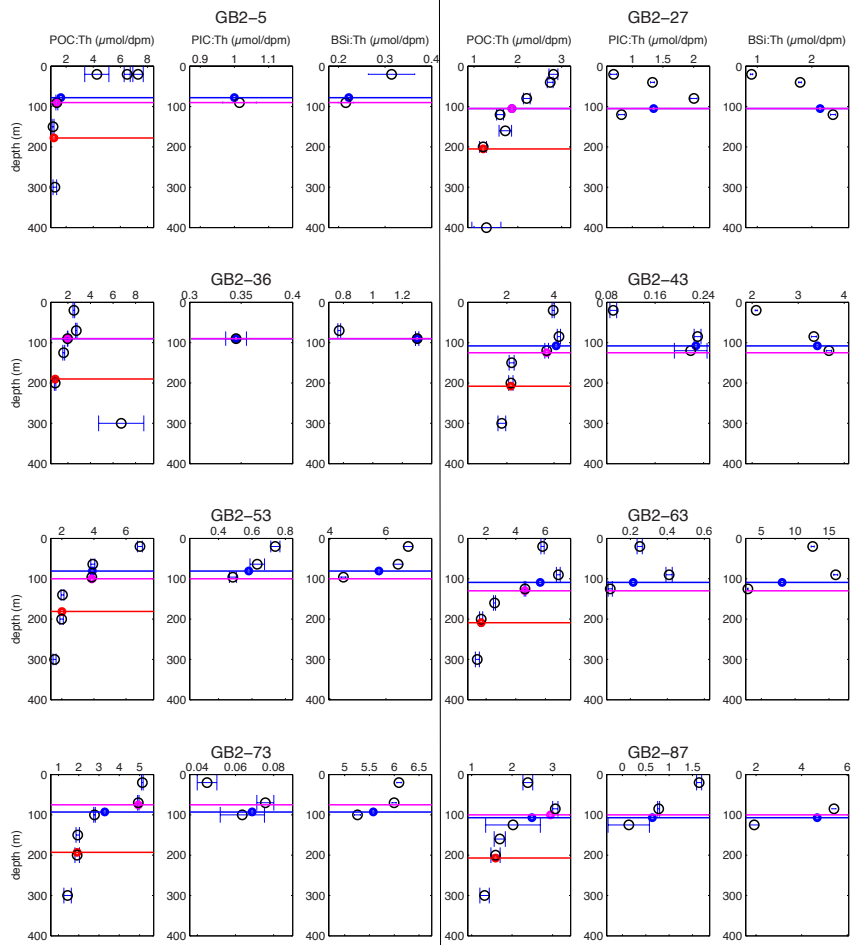
A



B



C



D

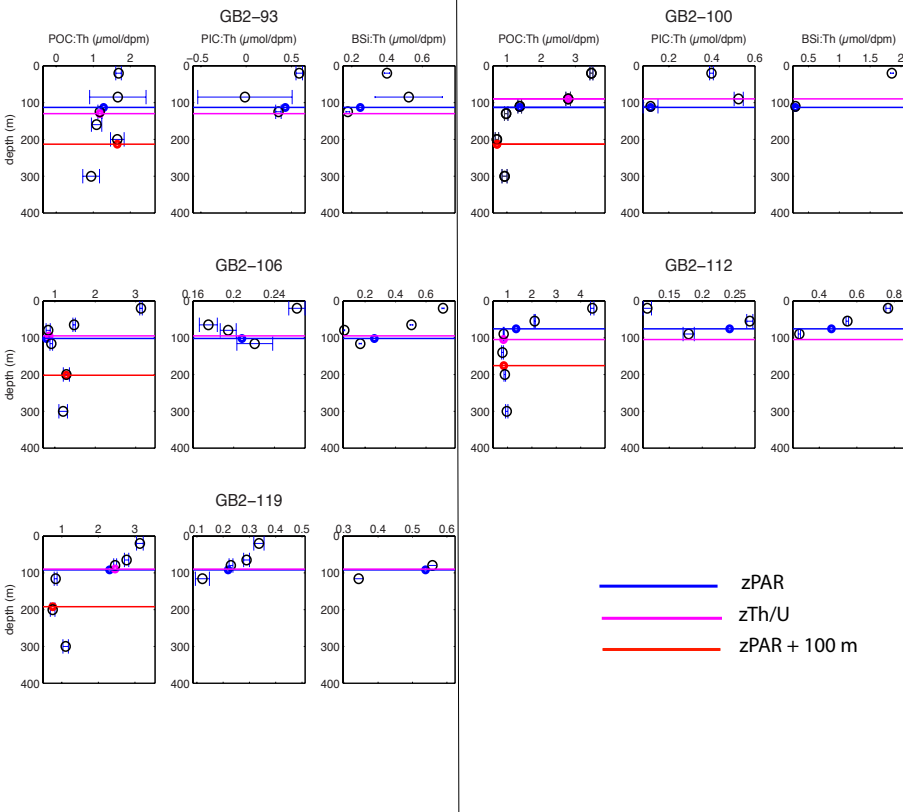


Figure S1. Profiles of $>51 \mu\text{m}$ POC: ^{234}Th , PIC: ^{234}Th and BSi: ^{234}Th above 400 m. Black open circles represent measurements. Colored circles represent values at three possible depths (colored lines; see legend) in the POC: ^{234}Th panels, and at z_{PAR} (blue line) for the PIC: ^{234}Th and BSi: ^{234}Th panels. These values were interpolated when there were no measurements at these depths (refer to Tables 2 and 3 for specific stations). At station GB2-106, the BSi: ^{234}Th interpolation calculation excluded the anomalously low value at 80 m. Error bars shown are the propagated errors of $>51 \mu\text{m}$ [POC], [PIC], [BSi] and particulate ^{234}Th activity measurements. Note that “negative” values are below the instrument detection limit (see Sect. 2.3), and are equal to 0 within error.

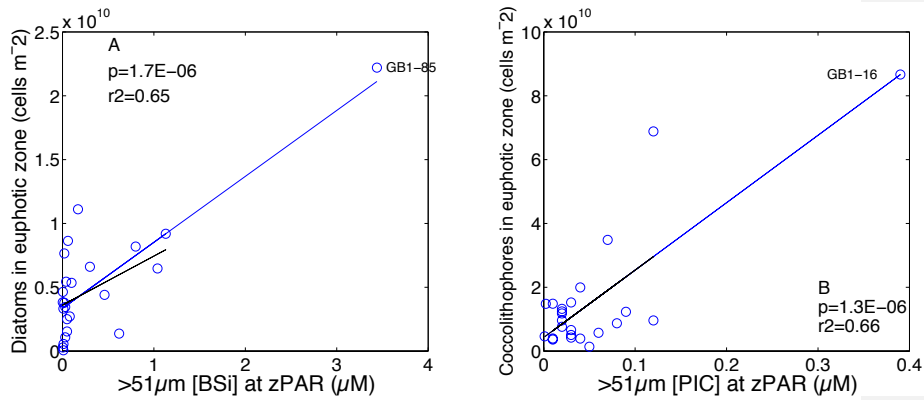


Figure S2. (A) Diatom cell counts integrated from surface to z_{PAR} (cells m^{-2}) as a function of $>51 \mu m$ [BSi] at z_{PAR} . (B) Integrated coccolithophore cell counts as a function of $>51 \mu m$ [PIC] at z_{PAR} . Outliers for $>51 \mu m$ [BSi] and [PIC] at stations GB1-85 and GB1-16, respectively, are defined according to Chauvenet's Theorem (Glover et al., 2011). Total euphotic zone cell counts of diatoms and coccolithophores are significantly correlated to $>51 \mu m$ [BSi] and [PIC] at z_{PAR} , respectively. The significant linear relationships are plotted here as blue lines, with corresponding p and r^2 values indicated. The regressions remain significant ($p < 0.05$) even when excluding the outliers GB1-85 (Fig. S2a) and GB1-16 (Fig. S2b) from analysis (black lines). We note that cell counts are only available for the $<36 \mu m$ size-fraction because of the methodology used for enumeration (see Supplemental Methods), while the biomineral measurements are of the $>51 \mu m$ particle size-fraction (Sect. 2.2). Nonetheless, these relationships suggest that the $>51 \mu m$ [BSi] and [PIC] at z_{PAR} do scale with the abundance of diatoms and coccolithophores in the euphotic zone of the water column.

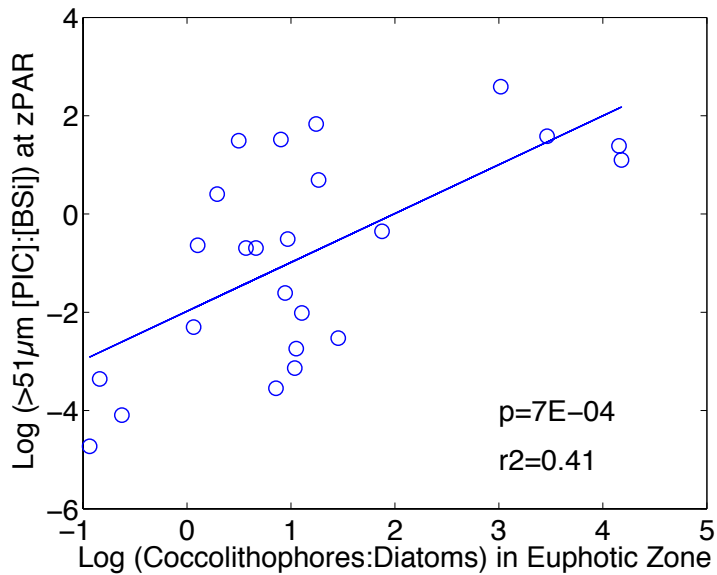


Figure S3. The natural log of the ratio of >51 μm [PIC]:[BSi] at z_{PAR} as a function of the natural log of the ratio of integrated coccolithophore: diatom cell counts in the euphotic zone. The significant linear relationship is plotted as a blue line, with a corresponding p and r^2 value indicated. This further supports the application of >51 μm size-fraction biomineral concentrations at z_{PAR} as a proxy for describing euphotic zone ecosystem composition in Sect. 4.7 and Fig. 10. Despite the different size-fractions that are represented by the biomineral measurements and the cell counts (see Supplemental Methods), the significant correlation nonetheless supports the use of >51 μm biomineral concentration ratios to describe the proportional abundance of certain phytoplankton types.

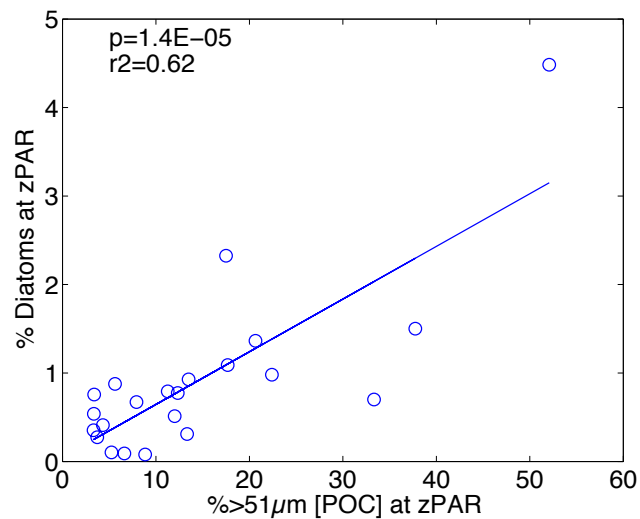


Figure S4. Percentage of total cells that are diatoms at z_{PAR} as a function of the % >51 μm [POC] at z_{PAR} . The significant linear relationship is plotted as a blue line, with a corresponding p and r^2 value indicated. This relationship shows that FlowCAM® measurements of diatom abundance support our interpretation that the size fractionation of POC (% >51 μm [POC] at z_{PAR}) determined from in-situ pump particle measurements (Sect. 2.2) reflects the relative abundance of diatoms. We note that there is no significant relationship between relative coccolithophore abundance and the size fractionation of POC.

Supplementary Methods for Figs. S2-S4

The FlowCAM® imaging cytometer enumerated nano- and microplankton cells from 10 mL Niskin cast samples at all McLane pump stations except GB2-36, GB2-27 and GB2-119 (refer to Table 1 for station locations) (Poulton and Martin, 2010). Moreover, at stations GB1-38 and GB1-70, cell counts were missing at z_{PAR} , and only measured at depths above and below z_{PAR} . The size range of counts was 5.6-35.5 μm . While particles $>36 \mu\text{m}$ (up to 200 μm) could be seen in the FlowCAM®, they were rare in 10 mL samples, such that their normalized abundance could not be accurately calculated. Total diatom cell counts in the euphotic zone were approximated by summing FlowCam® -derived diatom concentrations (cells/mL) at all depths above z_{PAR} :

$$\text{total cell counts} = \sum_1^{\text{end}} \text{mean} \left[\frac{\text{cells}}{\text{mL}}_n, \frac{\text{cells}}{\text{mL}}_{n-1} \right] \times [z_n - z_{n-1}]$$

where n is the measurement index number from the surface depth at $n=1$ downward towards z_{PAR} at $n=\text{“end”}$. The unit for this summation is equivalent to cells m^{-2} . Coccoliths and plated cells in the same Niskin samples were counted by birefringence microscopy (Balch et al., 2011). Total coccolithophore counts in the euphotic zone (cells m^{-2}) were similarly estimated by summing the microscopy-based concentrations at all depths above z_{PAR} .

Supplementary References

Balch, W. M., Drapeau, D. T., Bowler, B. C., Lyczkowski, E., Booth, E. S., and Alley, D.: The contribution of coccolithophores to the optical and inorganic carbon budgets during the Southern Ocean Gas Exchange Experiment: New evidence in support of the Great Calcite Belt hypothesis, *J. Geophys. Res.*, 116, C00F06, 2011.

Glover, D. M., Jenkins, W. J., and Doney, S. C.: *Modeling methods for marine science.*, Cambridge University Press, 2011.

Poulton, N. J., and Martin, J. L. Imaging flow cytometry for quantitative phytoplankton analysis - FlowCAM. In: Karlson B, Cusack C, Bresnan E (eds) *Microscopic and molecular methods for quantitative phytoplankton analysis*, Vol Chapter 8. Intergovernmental Oceanographic Commission of UNESCO, Paris, France, 49-54, 2010.